Water Research 206 (2021) 117727

Contents lists available at ScienceDirect

Water Research

journal homepage: www.elsevier.com/locate/watres

Photocatalytic ozonation in water treatment: Is there really a synergy between systems?

Manuel Figueredo, Eva M. Rodríguez *, Javier Rivas, Fernando J. Beltrán

Departamento de Ingeniería Química y Química Física, Instituto Universitario de Investigación del Agua, Cambio Climático y Sostenibilidad (IACYS), Universidad de Extremadura, Avda. Elvas S/N 06006, Badajoz, Spain

ARTICLE INFO

Keywords:
Photocatalytic ozonation
Synergy
High intensity UVA LEDs
Water matrix
Micropollutants and DOC removal

ABSTRACT

Numerous studies report on the synergy between ozonation and photocatalytic oxidation (TiO_2/UVA), which could open the way to the application of photocatalytic ozonation (PCOz) in water treatment. With the aim of establishing the existence of this synergy and its origin, in this work, using TiO_2 P25, 365 nm UVA LEDs and ozone transferred doses up to 5 mg (mg DOC_0)$^{-1}$ (DOC_0 7 – 10 mg L^{-1}), a systematic study has been carried out featuring the effect of pH, alkalinity and water matrix in each of the systems involved in PCOz, with special attention to the role of organics adsorption onto TiO_2. In ultrapure water, an increase in pH and carbonates content exerted a slight negative effect on the photocatalytic degradation of primidone (low adsorption onto TiO_2 and mainly abated by free $HO^{\bullet}$), this effect being higher on its mineralization. The negative effect of pH and alkalinity was much stronger for oxalic acid (high tendency to adsorb and mainly oxidized by positive holes). Accordingly, the results obtained at pH < pH_{pzc} (point of zero charge of the catalyst) in ultrapure water cannot at all be extrapolated to secondary effluents, since their composition negatively affects the photocatalytic performance. At the experimental conditions applied, only for the secondary effluent a synergy between O_3/UVA and TiO_2/UVA systems was observed. This synergy would be related, on the one hand, to the generation, from the matrix itself, of reactive entities or intermediates that promote the decomposition of ozone into $HO^{\bullet}$; and, on the other hand, to an increase in catalyst activity as the matrix UVA absorption decreases, rather than from direct interactions between both systems. Despite de above, ozone requirement to achieve a significant reduction of DOC is high and would only be an interesting strategy for the elimination of ozone-refractory micropollutants.

1. Introduction

1.1. TiO_2 photoexcitation. Background

Photoexcitation of TiO_2 in water generates positive holes (h^+) and $HO^{\bullet}$ at the catalyst surface, as well as $O_2^{\bullet-}$ and H_2O_2 (Nosaka and Nosaka, 2016, 2017). Since the redox potential of positive holes and surface $HO^{\bullet}$ is practically the same (Nosaka and Nosaka, 2016), both will be referred as h^+ in the present work. Surface $HO^{\bullet}$ can diffuse to the bulk (hereafter denoted as free $HO^{\bullet}$) and, when rutile phase is present (as it is the case of TiO_2 P25, anatase/rutile ratio 5.3 ± 0.28, Ohtani et al., 2010), H_2O_2 could also improve the release of $HO^{\bullet}$ through the formation of a peroxo-titanium complex and further cleavage of the O—O bond by h^+. Contrary to the classical mechanism accepted, the formation of $HO^{\bullet}$ from the reaction between H_2O_2 and e^- does not seem to be possible and must be disregarded (Nosaka and Nosaka, 2016). Accordingly, the amount of h^+ generated at the surface is higher than that of $HO^{\bullet}$ in the liquid bulk.

1.2. The role of the adsorption process on TiO_2 photocatalysis

Although any compound could react with free $HO^{\bullet}$, only those capable of being adsorbed on TiO_2 can interact with h^+, implying that h^+ is much more selective than free $HO^{\bullet}$. The adsorption of a given compound will depend on its structure and ionization state (pK_a) at the pH of the medium, together with the pH_{pzc} of the catalyst (point of zero charge), the latter being 6.3 – 6.9 for TiO_2 P25 (Kosmulski, 2009; Rosal et al., 2009; Perez Holmberg et al., 2013).

Literature includes numerous studies supporting the efficiency of the TiO_2/UVA system under acidic/slightly acidic conditions (that is, pH < pH_{pzc}) for the degradation of model contaminants and their mineralization in ultrapure water (Beltrán et al., 2008; Rodríguez et al., 2010;

* Corresponding author.
E-mail address: evarguez@unex.es (E.M. Rodríguez).

https://doi.org/10.1016/j.watres.2021.117727
Received 28 May 2021; Received in revised form 21 September 2021; Accepted 25 September 2021
Available online 30 September 2021
0043-1354/© 2021 The Author(s). Published by Elsevier Ltd. This is an open access article under the CC BY-NC-ND license (http://creativecommons.org/licenses/by-nc-nd/4.0/).

Tong et al., 2012; Moreira et al., 2015; Rimoldi et al., 2017; Jallouli et al., 2018), in many cases identifying $HO^{\bullet}$ and h^{+} as the main species responsible for the transformation of compounds with low or high tendency to be adsorbed on the catalyst, respectively. In terms of dissolved organic carbon (DOC) mineralization, if the conversion of final products (carboxylic acids, ketones, and aldehydes of low molecular weight) to CO_2 and H_2O relies, at least in part, in their adsorption and further oxidation by h^{+}, for final products with $pK_a < pH_{pzc}$ the mineralization efficiency will decrease at $pH > pH_{pzc}$, due to electrostatic repulsion. The presence of carbonates/bicarbonates (alkalinity) negatively affect DOC removal due to their adsorption and occupation of active centers and possible decrease of pH_{pzc} (Farner Budarz et al., 2017). Hence, having in mind the typical composition and characteristics of secondary effluents (SE) from municipal wastewater treatment plants (MWWTP), that is, $pH > pH_{pzc}$ P25 and medium/high alkalinity content, in SE the direct contribution of h^{+} to DOC mineralization is expected to be minimal.

1.3. Agglomeration/aggregation of catalyst particles during TiO_2 photocatalysis

SE composition could favor the agglomeration/aggregation (reversible/irreversible) of catalyst particles, negatively affecting the diffusion of $HO^{\bullet}$ (Ivanova et al., 2016). Although the role of salts commonly present in SE on the photocatalytic oxidation efficiency is controversial, Farner Budarz et al. (2017) reported that, at pH 7.9, Cl^{-}, $SO_4^{=}$, and NO_3^{-} (present in SE at relatively high concentrations) have low or no tendency to be adsorbed on TiO_2 but, even at concentrations as low as 0.5 mM, these anions can cause the significant aggregation of TiO_2 particles, decreasing the diffusion of $HO^{\bullet}$ to the liquid. Divalent cations as Ca^{2+} also favor the agglomeration/aggregation of TiO_2 particles whereas organic matter seems to contribute to their stabilization (Zhang et al., 2009).

1.4. Other effects of water matrix on TiO_2 photocatalysis

Although under 365 nm UVA radiation the photolysis of common ions in SE is not relevant, the organic matter of the effluent (EfOM) can absorb radiation and generate reactive species (Lee et al., 2013; Zhou et al., 2017). However, the attenuation of UVA radiation by the matrix can negatively affect the photoexcitation of the catalyst and hence the generation of h^{+} and free $HO^{\bullet}$. Moreover, depending on their concentration and reactivity, all the organics/inorganics present in SE may act as $HO^{\bullet}$ sink (Brame et al., 2015; Farner Budarz et al., 2017; Maghsoodi et al., 2019), or compete for catalyst active sites, diminishing the efficiency of the photocatalytic process.

1.5. Photocatalytic ozonation (PCOz). Background

Compared to TiO_2/UVA, several studies report the higher efficiency of the O_3/TiO_2/UVA system (photocatalytic ozonation, PCOz), both in the elimination of microcontaminants and reduction of DOC. During PCOz application, micropollutants are degraded through different mechanisms such as molecular ozone attack, direct/indirect photolysis and reaction with h^{+} and/or free $HO^{\bullet}$. Free $HO^{\bullet}$, generated through ozone decomposition, TiO_2 photoexcitation and even by EfOM photolysis, is usually considered the main responsible for the degradation of ozone refractory compounds and DOC elimination (Mehrjouei et al., 2015; Beltrán and Rey, 2017; Mecha and Chollom, 2020). As for TiO_2/UVA, the nature of the contaminants and the characteristics of the water matrix are key parameters in PCOz efficiency. Thus, working with model compounds in ultrapure water or without pH control (usually pH sharply decreases due to carboxylic acids formation) results in a process efficiency much higher than at higher pH, especially in terms of DOC mineralization (Beltrán et al., 2008; Márquez et al., 2014; Moreira et al., 2016; Jallouli et al., 2018; Lado Ribeiro et al., 2019). This influence of pH in PCOz could be related, at least in part, to an increase in the participation of h^{+} as the pH decreases and be misinterpreted as a synergy between systems. The potential synergy should be validated (respect to TiO_2/UVA and O_3/UVA) from experiments performed at the same conditions, with special attention to pH.

1.6. Synergy in PCOz

The synergy between simpler systems observed by different authors has been mainly attributed: *i)* to the role of ozone as scavenger of e^{-} at the catalyst surface, allowing the generation of $O_3^{\bullet-}$ and diminishing e^{-} - h^{+}recombination (Mehrjouei et al., 2015; Fathinia et al., 2016; Beltrán and Rey, 2017; Suligoj et al., 2021). However, although the reactivity of O_3 towards e^{-} is twice that of O_2 (3.6×10^{10} $M^{-1}s^{-1}$ *vs* 1.9×10^{10} $M^{-1}s^{-1}$, Bahnemann and Hart, 1982; Buxton et al., 1988), considering the much higher concentration of O_2 in the feeding gas and the higher solubility of O_2, e^{-} would be mainly captured by O_2 to form $O_2^{\bullet-}$, and *ii)* to the reaction between $O_2^{\bullet-}$ and O_3 leading to $O_3^{\bullet-}$, which seems more probable. Suligoj et al. (2021), from experiments performed at pH 3 using P25, concluded that the lower the adsorption of the compound onto the catalyst, the higher the synergy between systems, and this synergy also increased with the O_3 dose.

1.7. Objectives of the present work

In wastewater treatment, implementation of a tertiary advanced oxidation step may be needed for a safe discharge of the treated water and/or its reuse in periods of drought or water shortage. PCOz can be considered as one of these advanced processes, provided the existence of a synergy between ozonation and photocatalytic oxidation.

In a previous work (Figueredo et al., 2020), the application of PCOz on the degradation and mineralization of primidone (PRM) as probe compound in ultrapure water was studied. From the results obtained, a mechanism was proposed and applied at specific conditions, without considering the effect of matrix properties (pH, alkalinity, etc.).

The present work aims at identifying the existence of synergy between O_3/UVA and TiO_2/UVA on the elimination of pollutants and DOC. Although DOC reduction represents the importance of a full oxidation step, which is not the objective in a real MWWTP, this parameter can bring important information to clarify the existence of any synergy between O_3/UVA and TiO_2/UVA.

Primidone was selected as probe compound as it has no tendency to adsorb onto TiO_2 or photolyze under UVA. Oxalic acid (OXAL), a carboxylic acid usually detected in the final stages of organic matter oxidation, was also selected due to its high tendency to adsorb onto TiO_2, no UVA absorption, very low reactivity towards O_3 and relatively low reactivity with $HO^{\bullet}$. Aqueous solutions of both compounds and the secondary effluent from a MWWTP, spiked in some cases with different micropollutants with low/medium reactivity towards O_3 (PRM, caffeine, CAF; and p-chlorobenzoic acid, pCBA), were treated by TiO_2/UVA, O_3, O_3/UVA and O_3/TiO_2/UVA working at different pH and alkalinity content.

In an attempt to substantiate the effect of the operating parameters, it was tried to correlate different phenomena occurring, including adsorption, agglomeration/aggregation, role of holes and free radicals, etc., to the potential synergy of the PCOz system. Specific objectives were to assess: *i)* the effect of experimental conditions and water matrix on the removal of target compounds and DOC *ii)* the species and mechanisms involved, and *iii)* the existence of synergies between systems and parameters governing the synergy extent.

2. Experimental

2.1. Reagents

All the reagents and eluents used in this work (analytical grade and

HPLC-gradient grade, respectively), were obtained from Sigma-Aldrich, VWR and Fischer Scientific and used as received. TiO_2 P25 Aeroxide® was from Evonik Industries (Essen, Germany), ultrapure water produced by a Millipore Milli-Q® academic system (Darmstadt, Germany), and pressurized oxygen (purity > 99.5) supplied by Linde. Chemical structures, pK_a values and apparent second-order rate constant of the reaction of the selected compounds with $HO^\bullet$ and O_3 are shown in Table S1 (Supplementary information).

The secondary effluent (SE) came from the secondary decanter of the MWWTP Rincón de Caya (Badajoz, Spain), where a biological treatment based on an activated sludge process is applied. The SE was filtered (Whatman grade 1) and frozen until use. Main characteristics of the SE are given in Table S2 (Supporting information).

2.2. Experimental setup

The experimental set-up (see Fig. S1) has been previously described (Figueredo et al., 2020). Briefly, it consisted of an agitated tank (borosilicate glass, 1.3 L capacity, magnetic stirring) with inlets/outlets for gasses and sampling. The tank was initially filled with 1 L of the water to be treated and then pumped (peristaltic pump, Q_L 7.7 L h^{-1}) to a tubular photoreactor (borosilicate glass, 50 cm long, 2.8 cm internal diameter, total volume 0.36 L) in recirculation mode. The tube was permanently covered by a stainless-steel reflector. As radiation source 6 LEDs (LZ4-04UV00, LED ENGIN; ~ 3 W radiant power each, λ_{max} 365 nm) located under the glass tube were used. Using nitrite as actinometer, a photon flux of 3.92×10^{-5} Einstein (L s)$^{-1}$ reaching the liquid was determined (Figueredo et al., 2020).

In a typical experiment using TiO_2, the whole installation was draped by aluminum foil, the tank filled, a sample taken, and the catalyst added (10 – 500 mg L^{-1}). Then, the stirring and pumping systems were turned on and the O_2 stream (Q_g 15 L h^{-1}) fed to the tank through a glass diffuser. After 30 min (adsorption period in the dark) a new sample was taken ($t = 0$ min), the aluminum foil removed and the LEDs switched on, then taking samples at different times. A similar procedure was followed when ozone was used, starting the O_2/O_3 bubbling in the ozonation tank (Q_g 15 L h^{-1} and $[O_{3g,in}]$ 10 mg L^{-1}) once the photoreactor was filled (single ozonation), the LEDs were switched on (photolytic ozonation, O_3/UVA), or after the adsorption period in the dark (photocatalytic ozonation). Considering the gas flow rate, the concentration of O_3 in the gas inlet and outlet, the reaction volume and the initial DOC content, the evolution of transferred ozone dose (TOD) per unit of DOC_0 (TOD/DOC_0, mg O_3 (mg DOC_0)$^{-1}$) was determined. In all cases, ozone transferred doses up to ~ 5 mg O_3 (mg DOC_0)$^{-1}$ in 2 h were applied.

According to the installation design, the concentration of ozone entering the photoreactor at a given time corresponds to the dissolved ozone present in the tank. As will be seen later, this configuration will be useful to determine the interactions between systems. All the experiments were carried out at room temperature. After 2 h (total reaction time) the increase in temperature was less than 2 °C.

In experiments using PRM, CAF and/or pCBA as probe compounds, concentrated solutions were prepared in ultrapure water, then adding the volume needed to obtain the desired concentration in 1 L final volume (PRM 14 mg L^{-1} in ultrapure water; PRM, CAF and pCBA 100 μg L^{-1} each in SE). When OXAL was used as probe compound, the working solution (35 mg L^{-1} of $C_2H_2O_4\bullet2H_2O$ in ultrapure water) was directly prepared before the experiment.

In experiments in the presence of tert-butanol (tBuOH) 0.1 M as $HO^\bullet$ scavenger, 10 mL of pure tBuOH were added to 1 L of the reaction medium.

When needed, some drops of concentrated NaOH or $HClO_4$ were added to correct the initial pH. $HClO_4$ was also used to remove inorganic carbon (IC) from SE. In experiments in ultrapure water in the presence of IC (30 mg L^{-1}), pH was first corrected to 7.5 with NaOH, the required amount of $NaHCO_3$ added, and the pH corrected to pH 8.4 if needed.

2.3. Analytical methods

The concentration of ozone in the gas streams (inlet/outlet) was monitored by an Anseros Ozomat GM-6000 Pro analyzer. PRM, CAF and pCBA concentration were analyzed by HPLC (Agilent 1100 Series) with UV–Vis detector, using a Kromasil C18 column (150×4 mm, 100 Å pore size, 5 μm particle size). Inorganic anions and short-chain organic acids were analyzed by ion chromatography with chemical suppression (Metrohm 881 Compact Pro) and conductivity detection, using a MetroSep A Supp 7 column (4 × 150 mm, 5 μm). The description of the chromatographic methods and the limits of detection (LOD) and quantitation (LOQ) are given in Text S1. The concentration of DOC and IC in water was determined using a Shimadzu TOC-VSCH analyzer and the concentration of ozone and hydrogen peroxide by the indigo method (Bader and Hoigné, 1981) and cobalt-bicarbonate method (Masschelein et al., 1977), respectively. $N—NH_4^+$ was determined using a Spectroquant® test kit (Merck), COD and N_{Total} using Hach Lange test kits, and BOD_5 using an OxiTop® device. Spectrophotometric measurements were performed by means of an UV–Vis Evolution 201 (Thermo Scientific) spectrophotometer. After purging dissolved ozone (if present) with air, the samples were filtered (0.45 μM, PVDF Millipore) and analyzed.

2.4. Kinetic data processing

When the photocatalytic oxidation of an aqueous contaminant (C) mainly develops through its reaction with $HO^\bullet$, and, additionally, no direct photolysis occurs, degradation kinetics can be modelled by a simple pseudo-first order kinetics (Krýsa et al., 2006). Pseudo-first order kinetics is far away from considering the actual mechanism, but it is a useful tool for comparison purposes. Accordingly, the following equation applies:

$$\mathrm{Ln}\left(\frac{[C]}{[C]_0}\right) = -k_{Obs-C}\cdot t \quad (1)$$

where:

$$k_{Obs-C} = k_{C-HO^\bullet}[HO^\bullet]_{ss} \quad (2)$$

In Eq. (1) $k_{Obs\text{-}C}$ stands for the observed pseudo-first order rate constant (s^{-1}), $k_{C\text{-}HO^\bullet}$ is the second order rate constant of the reaction between the compound C and $HO^\bullet$ (M^{-1} s^{-1}), and $[HO^\bullet]_{ss}$ represents the average molar concentration of hydroxyl radicals under steady state conditions.

If concentration data of C versus time and $k_{C\text{-}HO^\bullet}$ are known, Eqs. (1) and (2) allow $k_{Obs\text{-}C}$ and $[HO^\bullet]_{ss}$ to be determined. These two parameters give a measure of the efficiency in $HO^\bullet$ generation as a function of the operating conditions applied.

Similarly, regardless of the species involved in the process (h^+ and/or $HO^\bullet$), the mineralization of contaminants can also be assumed to follow pseudo-first order kinetics. This hypothesis is applicable when the adsorption stage (in case it takes place) follows the Langmuir-Hinshelwood model and the DOC content is sufficiently low (Krýsa et al., 2006):

$$\mathrm{Ln}\left(\frac{[DOC]}{[DOC]_0}\right) = -k_{Obs-DOC}\cdot t \quad (3)$$

where [DOC] is the concentration of DOC and $k_{Obs\text{-}DOC}$ the observed pseudo-first order rate constant.

3. Results and discussion

3.1. Photocatalytic oxidation using TiO_2 P25 and UVA LEDs

3.1.1. Primidone. The role of free $HO^\bullet$ radicals

In a first experimental series PRM was used as a model compound in ultrapure water, using different P25 doses under continuous bubbling of

pure oxygen. Alkalinity and pH effects were also studied to understand the main features governing the process.

According to a previous work (Figueredo et al., 2019), the initial photocatalytic transformation of PRM in the presence of TiO_2 P25 is mainly caused by its reaction with free $HO^{\bullet}$. In addition, as experimentally proven, the photolysis of PRM under 365 nm radiation provided by LEDs and its adsorption on TiO_2 are negligible.

Fig. 1a shows $k_{Obs\text{-}PRM}$ values obtained after fitting the experimental results to Eq. (1), and the stationary hydroxyl radical concentration $[HO^{\bullet}]_{ss}$ (Eq. (2)). Fig. 1b displays the values of $k_{Obs\text{-}DOC}$ (Eq. (3)). The fitting process is shown in Figs. S2 and S3, and pH evolution in Fig. S4.

At $pH_0 \sim 6$ (pH gradually decreased to 4.7 after 2 h, Fig. S4), as inferred from Fig. 1a, an increase in TiO_2 load from 10 to 250 mg L^{-1} led to an exponential increase in free $HO^{\bullet}$ production, with estimated $[HO^{\bullet}]_{ss}$ and $k_{Obs\text{-}PRM}$ values ranging from 5×10^{-14} M to 2.5×10^{-13} M, and from 0.017 min^{-1} to 0.100 min^{-1}, respectively. No further improvement at higher TiO_2 doses was experienced. At the experimental conditions applied, from PRM initial removal rates (that is, assuming there is no $HO^{\bullet}$ consumption by intermediates), a maximum apparent efficiency of $\sim$ 0.002 mol $HO^{\bullet}$ (Einstein)$^{-1}$ was estimated, the optimal catalyst dose in ultrapure water being in the proximity of 100 mg L^{-1} (see Text S2).

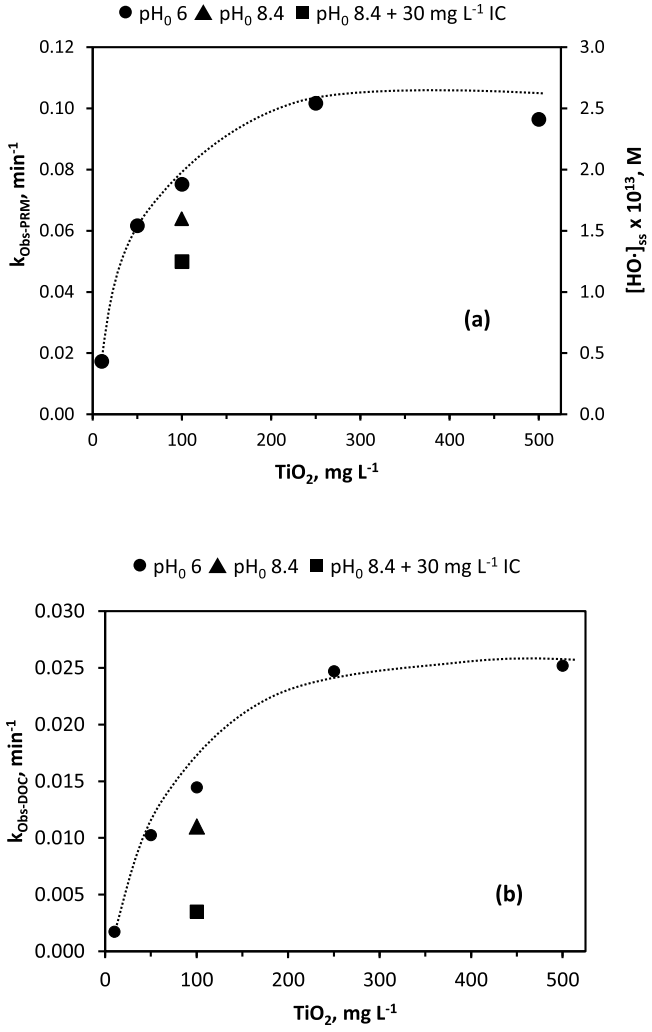

Fig. 1. PRM degradation by TiO_2/UVA LEDs in ultrapure water. Influence of catalyst dose, pH and IC content on: (a) $k_{Obs\text{-}PRM}$ (Eq. (1)) and $[HO^{\bullet}]_{ss}$ (Eq. (2)); (b) $k_{Obs\text{-}DOC}$ (Eq. (3)). Experimental conditions: $[PRM]_0$ 14 mg L^{-1} ($\sim 6.5 \times 10^{-5}$ M), $[DOC]_0$ 9 mg L^{-1}, Q_g 15 L h^{-1}, $I_{0,365\ nm} = 3.92 \times 10^{-5}$ Einstein (L s)$^{-1}$, $T = 20 \pm 2$ °C.

Regarding mineralization (Fig. 1b) at pH_0 6, catalyst doses from 10 to 250 mg L^{-1} led to $k_{Obs\text{-}DOC}$ from 0.0017 min^{-1} to 0.025 min^{-1}, DOC reduction ranging from 20% to 95% after 2 h (Fig. S3). Again, there was no further improvement in $k_{Obs\text{-}DOC}$ at higher titania doses. According to the values shown in Fig. 1a and b, at pH_0 6 the ratio $k_{Obs\text{-}DOC}/k_{Obs\text{-}PRM}$ increased with the catalyst dose from 0.1 (10 mg L^{-1}) to 0.23 (250–500 mg L^{-1}). Hence, the positive effect of the amount of catalyst is higher in PRM mineralization than in its initial transformation, which suggests the development of different oxidation mechanisms.

Compared to measurements conducted at $pH_0 \sim 6$ with 100 mg L^{-1} of TiO_2, an increase of initial pH to 8.4 led to a decrease in $k_{Obs\text{-}PRM}$ of roughly 15% in the absence of IC and 35% when 30 mg L^{-1} of IC were added. Since the effect of PRM speciation can be disregarded (PRM pK_a 11.5), the slight negative effect of pH and alkalinity in $[HO^{\bullet}]_{ss}$ would be related to the influence of both parameters in the agglomeration/aggregation of P25 particles (Autin et al., 2013; Jefferson et al., 2016; Li et al., 2016; Wang, 2017) and/or occupation of active sites by carbonates/bicarbonates. Additionally, alkalinity may act as $HO^{\bullet}$ scavenger, consequence of the following equilibria and reactions (Buxton and Elliot, 1986; Real et al., 2009):

$$H_2CO_3 \overset{pKa=6.34}{\leftrightarrows} H^+ + HCO_3^- \overset{pKa=10.37}{\leftrightarrows} 2H^+ + CO_3^= \quad (4)$$

$$HCO_3^- + HO^{\bullet} \xrightarrow{k=8.5\times10^6\ M^{-1}s^{-1}} CO_3^{\bullet-} + H_2O \quad (5)$$

$$CO_3^= + HO^{\bullet} \xrightarrow{k=4.2\times10^8\ M^{-1}s^{-1}} CO_3^{\bullet-} + OH^- \quad (6)$$

$$PRM + HO^{\bullet} \xrightarrow{k=6.7\times10^9\ M^{-1}s^{-1}} Intermediate \quad (7)$$

According to equilibria (4), at pH_0 8.4 IC is mainly present as HCO_3^-. Considering the initial concentrations of PRM and HCO_3^-, together with the values of the second order rate constant of their reaction with $HO^{\bullet}$, approximately 95% of $HO^{\bullet}$ should be captured by PRM, so the scavenging effect of HCO_3^- on $k_{Obs\text{-}PRM}$ would be negligible.

The increase of the initial pH from 6 to 8.4 also caused a reduction of $\sim$ 22% in $k_{Obs\text{-}DOC}$, similar to the 15% decrease in $k_{Obs\text{-}PRM}$. The negative effect of pH was significantly amplified in the presence of 30 mg L^{-1} IC, with a $k_{Obs\text{-}DOC}$ reduction of 75%, twice that of $k_{Obs\text{-}PRM}$ (35%). The fact that the effect of alkalinity is more pronounced in PRM mineralization than in its initial transformation suggests either the refractory character of some of the intermediates towards $HO^{\bullet}$ (not being able to compete with HCO_3^-) and/or, again, that the species involved in both processes differ. Thus, given the high tendency of carbonates/bicarbonates to adsorb onto TiO_2 (Dolamic and Bürgi, 2007; Farner Budarz et al., 2017), they could inhibit/decrease the development of oxidation reactions involving h^+ and their contribution to mineralization.

Fig. 2a shows the generation/evolution of some low molecular weight carboxylic acids and dissolved inorganic nitrogen (DIN) in solution (i.e. $N—NH_4^+$ and $N—NO_3^-$; $N—NO_2^-$ remained below the LOD), for runs at pH_0 6 after reaching different DOC conversions. As observed, formic (FOR), oxalic (OXAL) and acetic (ACE) acids were the main carboxylic acids detected. After an initial increase, acids concentration gradually decreased with DOC conversion while DIN increased, mainly in the form of $N—NH_4^+$ (see also Text S3). The low conversion of $N—NH_4^+$ to $N—NO_3^-$ would be the result of its low adsorption onto TiO_2 (absence of oxidation by h^+) and low reactivity towards free $HO^{\bullet}$ (Buxton et al., 1988; Bonsen et al., 1997; Zhu et al., 2005; Huang et al., 2008).

Fig. 2b shows the influence of pH and alkalinity on the concentration of low molecular weight carboxylic acids and DIN in solution after reaching 35 - 40% DOC removal. Compared to the run at pH_0 6 (no IC), the results clearly reveal the high accumulation of OXAL in solution when the initial pH was set at 8.4 and 30 mg L^{-1} of IC were added.

3.1.2. *Oxalic acid. The role of holes*

In view of the previous results, a series of OXAL photocatalytic

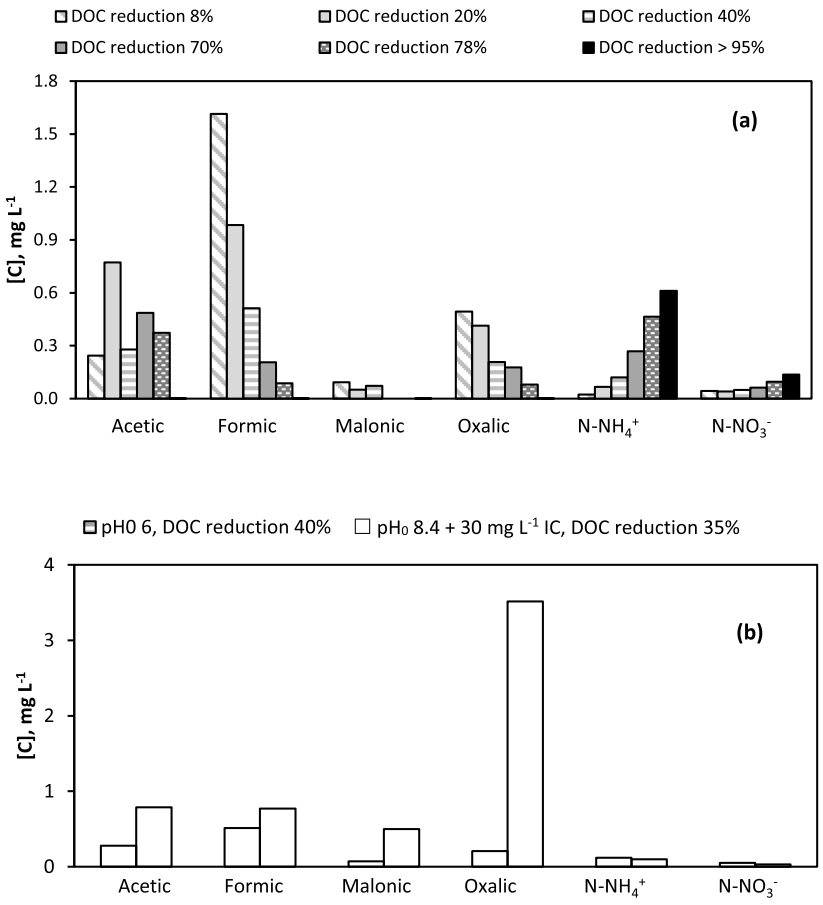

Fig. 2. Formation of carboxylic acids and DIN species from PRM degradation by TiO_2/UVA LEDs in ultrapure water. (a) Influence of DOC reduction achieved at pH_0 6; (b) influence of pH_0 and IC content for a 35–40% of DOC reduction. Experimental conditions: $[PRM]_0$ 14 mg L^{-1} (~ 6.5 × 10^{-5} M), $[DOC]_0$ 9 mg L^{-1}, Q_g 15 L h^{-1}, $[TiO_2]$ 100 mg L^{-1}, $I_{0,}365_{nm}$ = 3.92×10^{-5} Einstein (L s)$^{-1}$, T = 20 ± 2 °C.

oxidation experiments was completed. OXAL (pK_{a1} 1.25 and pK_{a2} 4.27, Mendive et al., 2007) presents relatively low reactivity towards $HO^{\bullet}$ (see Table S1), and high tendency to be adsorbed onto TiO_2 forming mono and bidentate surface complexes (Hug and Sulzberger, 1994; Weisz et al., 2002; Park et al., 2006; Mendive et al., 2007). The reaction of OXAL with h^+ is accepted to be the principal photocatalytic pathway under UV radiation (Krýsa et al., 2006; Schneider et al., 2020) leading to CO_2 and $CO_2^{\bullet-}$, the latter evolving to CO_2 and $O_2^{\bullet-}/HO_2^{\bullet}$ in the presence of dissolved O_2 (Krýsa et al., 2006). As a consequence, OXAL is directly converted to CO_2 (and/or bicarbonate/carbonate depending on pH) so $k_{Obs\text{-}OXAL}$ and $k_{Obs\text{-}DOC}$ values are the same. Given the high OXAL capability of adsorption and reaction with h^+, the specialized bibliography includes numerous works in which OXAL is used as a h^+scavenger (Kominami et al., 2001; Rodríguez et al., 2015; Schneider et al., 2020).

Tests were carried out in ultrapure water with initial pH fixed at 3.5, 6 and 8.4. In the latter case the influence of IC addition was also investigated. To determine the possible participation of free $HO^{\bullet}$ in the degradation of OXAL, experiments were also performed in the presence of tBuOH 0.1 M, alcohol concentration high enough to scavenge $HO^{\bullet}$ ($k_{tBuOH—HO\bullet}$ 6.2 × 10^8 M^{-1} s^{-1}, Alam et al., 2003). Due to tBuOH low adsorption and capacity to act as electron donor, h^+ generation should not be affected (Kim et al., 2014; Burek et al., 2019).

Fig. 3a shows the evolution of the normalized concentration of OXAL with time (solid lines are fitting to Eq. (1)) and Fig. 3b the pH variation. In all cases, the amount of OXAL adsorbed onto TiO_2 after an initial period of 30 min in the dark was undetectable, in line with the adsorption isotherm determined by Ivanova et al. (2016) at pH 3.7 and 25 °C (predicted OXAL adsorbed < 6 μM). Under the conditions tested, the concentration of H_2O_2 in solution was below 5 × 10^{-6} M (not shown).

At pH_0 3.5, and as reported in the literature (Kosanić, 1998; Orge et al., 2015), OXAL elimination rate was significantly high ($k_{Obs\text{-}OXAL}$ > 0.07 min^{-1}) being fully converted in less than 30 min (Fig. 3a). At this pH the surface of the catalyst is positively charged and OXAL mainly on its monoprotonated form (see speciation in Fig. S5), so the adsorption of OXAL and its h^+ oxidation is favored. Since the presence of 0.1 M tBuOH at pH_0 3.5 had no effect on OXAL elimination the participation of free $HO^{\bullet}$ can be ruled out.

At pH_0 6 ($k_{Obs\text{-}OXAL}$ 0.0071 min^{-1}; R^2 0.98), the attraction between OXAL and the TiO_2 surface is still favored. However, as the reaction progresses, the accumulation of $HCO_3^-/CO_3^=$ leads to a pH increase (Fig. 3b), called causticization by Wang and Adesina (1997), and the net positive charge of the catalyst decreases. Therefore, the electrostatic attraction between OXAL-TiO_2 P25 diminishes resulting in lower adsorption.

A further rise of initial pH to 8.4 (OXAL present as $C_2O_4^=$; $k_{Obs\text{-}OXAL}$ 0.0026 min^{-1}; R^2 0.98), results in a low initial degradation followed by a slight increase due to the pH drop to 7.5. At pH 8.4, the addition of 30 mg L^{-1} of IC implied no OXAL conversion after 2 h. Absence of mineralization is attributable to the occupation of active adsorption centers by $HCO_3^-/CO_3^=$ together with the role of IC as $HO^{\bullet}$ scavenger.

In summary, from Fig. 3 it is deduced that both pH and IC content have a strong negative impact on OXAL degradation by TiO_2/UVA. Surprisingly, at pH_0 > pH_{pzc}, presence of 0.1 M tBuOH favored the elimination of OXAL, effect that was significantly reduced in the presence of 30 mg L^{-1} of IC. Since the presence of tBuOH did not practically affect the evolution of pH (Fig. 3b), these results indicate that 0.1 M tBuOH enhanced somehow OXAL degradation. It is hypothesized that,

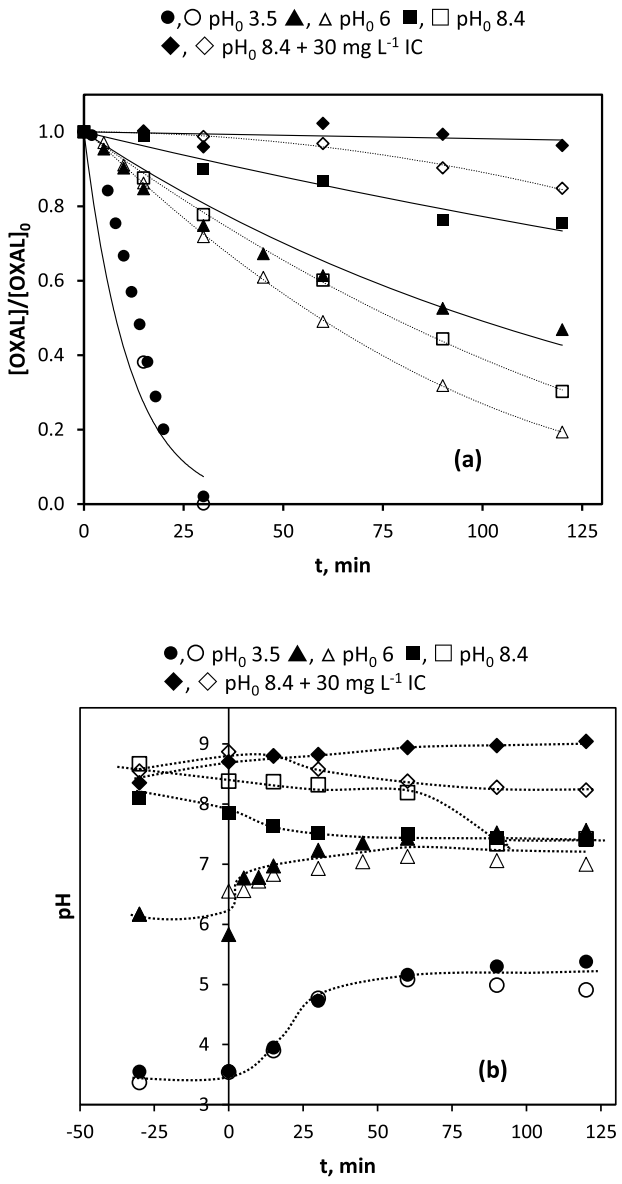

Fig. 3. OXAL degradation by TiO_2/UVA LEDs in ultrapure water. Influence of pH_0, IC content and presence of tBuOH on OXAL (a) and pH (b) evolution with time. Symbols: Experimental data in absence (solid) or presence (open) of 0.1 M tBuOH. Solid lines: fitting to Eq. (1) (absence of tBuOH). Experimental conditions: $[OXAL]_0$ 3×10^{-4} M, $[DOC]_0 \sim 7$ mg L^{-1}, $[TiO_2]$ 100 mg L^{-1}, Q_g 15 L h^{-1}, $I_{0,365\ nm} = 3.92 \times 10^{-5}$ Einstein $(L\ s)^{-1}$, $T = 20 \pm 2$ °C.

as the pH increases (and the adsorption of OXAL decreases), given the high concentration of the alcohol a small amount of tBuOH can be adsorbed and oxidized at the catalyst surface (oxidation by free hydroxyl radicals is not discarded), leading to radical species capable of degrading OXAL. The mechanism should be similar to that proposed by Cederbaum et al. (1983), based on the formation of the hydroxyalkyl or alkoxyl radicals. The spontaneous fission of the latter would lead to the methyl radical, which can attack a suitable electron donor or combine with oxygen to generate the methyl peroxy radical. Any of these species could react with OXAL. In the presence of IC, adsorption of tBuOH would be reduced.

Unlike OXAL, PRM mineralization requires previous oxidation steps. However, if $k_{Obs\text{-}DOC}$ values of PRM Fig. 1b) and OXAL (Fig. 3a) are compared for experiments at pH_0 8.4, PRM is more efficiently mineralized than OXAL in absence/presence of IC. This means that the oxidation/mineralization of low molecular weight intermediates other than OXAL formed during PRM photocatalytic degradation depends to a lesser extent on h^+, due to their higher reactivity with free $HO^\bullet$ or even with the $CO_3^{\bullet-}$ generated from reactions ((5) and (6). This is for example the case of FOR (pk_a 3.74, $k_{HO\bullet-HCO2-}$ 3.9×10^9 $M^{-1}s^{-1}$, Buxton et al., 1988; $k_{FOR\text{-}CO3\bullet-}$ 1.1×10^5 M^{-1} s^{-1}, Neta et al., 1988), that is oxidized to CO_2 and $O_2^{\bullet-}/HO_2^\bullet$ (Yapsakli and Can, 2004).

Attending to the results obtained working with PRM and OXAL, at $pH > pH_{pzc}$ the efficiency of the TiO_2/UVA system in DOC removal will be low, especially in the presence of alkalinity, due to the low contribution of h^+. Having in mind the importance of the adsorption process in the photocatalytic mechanism, a secondary effluent from a MWWTP was next considered. *A priori*, given the characteristics of these effluents, free $HO^\bullet$ is expected to be the main species involved in the oxidation and mineralization of the EfOM by this system.

3.1.3. *Secondary effluent from a MWWTP. Influence of the water matrix*

TiO_2/UVA system was applied to treat the SE from a MWWTP (see Table S1), doped with 100 μg L^{-1} of PRM and CAF as representative of micropollutants. Like PRM, CAF photocatalytic degradation is mainly caused by reaction with free $HO^\bullet$ (Dalmázio et al., 2005; Chuang et al., 2011), $k_{CAF\text{-}HO\bullet}$ being 5.9×10^9 M^{-1} s^{-1} (Shi et al., 1991). Another experiment was conducted under similar conditions previously eliminating the IC content by successive changes in pH. A first acidification stage led to IC removal and partial solubilization of suspended organic carbon (increase of DOC_0 from 10 to 12 mg L^{-1}), whereas the subsequent rise of pH led to an increase of 6 mg L^{-1} of residual IC due to CO_2 absorption. Regardless of the IC content, the pH of the effluent remained virtually constant along the treatment.

Fig. 4 compares the values of $k_{Obs\text{-}DOC}$ for SE (see variation of normalized DOC over time and fittings to Eq. (3) in Fig. S6) with those corresponding to PRM and OXAL in ultrapure water under similar conditions. The evolution of the normalized concentration of spiked PRM and CAF throughout SE photocatalytic treatment without/with IC removal is shown in Fig. 4b.

As observed in Fig. 4a, after 2 h, SE mineralization was negligible. In fact, a slight increase in DOC over time could be likely due to the solubilization of suspended matter (Fig. S6). The reduction of IC_0 content in SE had a slight positive effect on DOC removal (12% after 2 h) and carboxylic acid generation (see Fig. S7a). Due to the pH and IC content of the SE, the contribution of surface reactions to the oxidation of organics would be minimal. Besides, the agglomeration/aggregation of the catalyst in SE would be much higher than in ultrapure water, lowering the amount of $HO^\bullet$ that diffuses into the bulk.

Regarding the evolution of the normalized concentration of PRM and CAF (Fig. 4b), their profiles were similar regardless of the specific compound and IC content, reaching ~ 50% conversion after 2 h. This means that IC did not alter the production of $HO^\bullet$ nor competes with the micropollutants for $HO^\bullet$ or this was balanced by the formation of $CO_3^{\bullet-}$ (Wojnárovits et al., 2020). Fitting of experimental data to Eq. (1) lead to an average value of 0.008 min^{-1} for $k_{Obs\text{-}C}$, a sixth fold decrease if compared to the value of 0.05 min^{-1} obtained for PRM in ultrapure water at similar conditions. Hence, organics and inorganics other than $HCO_3^-/CO_3^=$ present in SE are responsible for the low $[HO^\bullet]_{ss}$ by acting as $HO^\bullet$ sink and/or lowering $HO^\bullet$ diffusion due to the agglomeration/aggregation of the catalyst. The latter phenomena have been reported in the presence Ca^{2+} (Zhang et al., 2009), Cl^-, $SO_4^=$, and NO_3^- (Farner Budarz et al., 2017) at concentration levels similar to those commonly found in MWWTP SE.

From the above results, the optimal catalyst dose in SE is probably higher than in ultrapure water. Thus, when 100 and 500 mg L^{-1} of TiO_2 were used, although in both cases there was no DOC removal after 2 h, a clear increase in the formation rate of carboxylic acids in solution was observed for the highest catalyst dose (Fig. S7b). In any case it could be deduced by the results that the application of TiO_2/UVA system in ultrapure water using probe compounds cannot be extrapolated at all to actual secondary effluents.

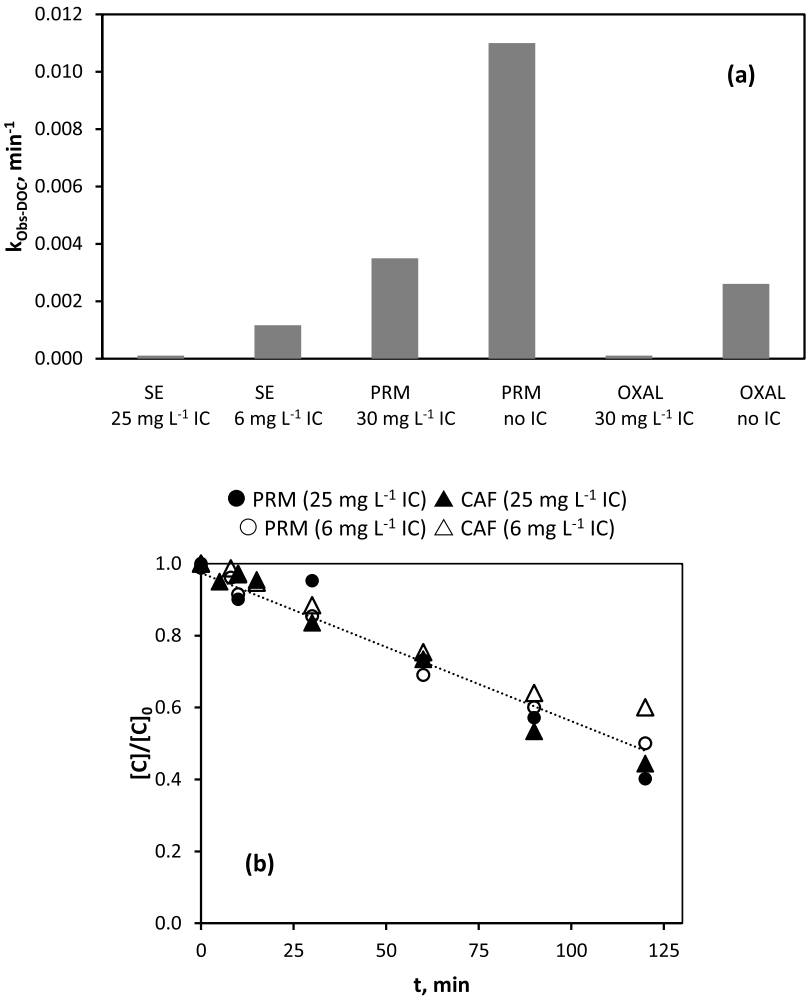

Fig. 4. (a) Influence of type of water matrix and IC content on $k_{Obs-DOC}$ (Eq. (3)) obtained by TiO_2/UVA LEDs; (b) influence of IC content on the photocatalytic removal of PRM and CAF (100 μg L^{-1} each) from SE. Experimental conditions: $[DOC\text{-}OXAL]_0 \sim 7$ mg L^{-1}, $[DOC\text{-}PRM]_0 \sim 9$ mg L^{-1}, $[DOC\text{-}SE]_0$ 10 - 12 mg L^{-1}, pH_0 8.2 - 8.4, $[TiO_2]$ 100 mg L^{-1}, Q_g 15 L h^{-1}, $I_{0,365\ nm} = 3.92\times10^{-5}$ Einstein (L s)$^{-1}$, $T = 20 \pm 2$ °C.

3.2. Photocatalytic ozonation using TiO_2 P25 and UVA LEDs

To determine the influence of water matrix characteristics on the effectiveness of PCOz technology and the potential existence of synergism between systems, a similar study was carried out by applying O_3, O_3/UVA and O_3/TiO_2/UVA.

3.2.1. Primidone

Ozone based systems were applied to degrade PRM in ultrapure water pH_0 6. PCOz was carried out also at pH_0 8.4 in the absence/presence of IC. During PCOz at pH_0 8.4 and no IC, the quick formation of acidic compounds and the lack of buffering capacity led to a fast pH decrease, so the results obtained were practically identical to those registered at pH_0 6 (not shown). This reflects the importance of this parameter when trying to determine the existence of real synergies between systems.

Fig. 5 shows $k_{Obs-PRM}$ (Fig. 5a) and $k_{Obs-DOC}$ (Fig. 5b) values obtained after fitting the data to simplistic pseudo-first order kinetics (see Fig. S8). For comparison purposes, data corresponding to the TiO_2/UVA system are also included. In Fig. 5a and Fig. 5b, dotted lines correspond to the sum of k_{Obs} values corresponding to O_3/UVA and TiO_2/UVA. Fig. 5c compares the evolution of PRM, DOC and dissolved ozone concentrations in the ozonation tank during PCOz tests performed at pH_0 6 (no IC) and 8.4 (30 mg L^{-1} of IC). The evolution of pH during all these runs is shown in Fig. S9.

Although the reactivity of PRM with ozone is relatively low ($k_{PRM\text{-}O3}$ 3 M^{-1} s^{-1}, Figueredo et al., 2019), the degradation of PRM by O_3 occurs through reaction with $HO^{\bullet}$ generated from ozone decomposition promoted by PRM itself (Figueredo et al., 2019). Therefore, as seen in Fig. 5a, under slightly acidic conditions the efficiency of O_3 and O_3/UVA systems was high and similar, with 90% PRM converted in less than 20 min. Values of $k_{Obs-PRM}$ from PCOz coincided with the sum of contributions from O_3/UVA and TiO_2/UVA systems (regardless of TiO_2 dose), so no synergy (or antagonism) is envisaged. As for TiO_2/UVA, the influence of pH and alkalinity on $k_{Obs-PRM}$ by PCOz was low (Fig. 5a).

In terms of mineralization (Fig. 5b), at pH_0 6 the effectiveness of simple ozonation was very low (10% DOC removal after 2 h). The ozone recalcitrance of carboxylic acids, ketones and aldehydes of low molecular weight (von Sonntag and von Gunten, 2012), makes necessary the participation of species with higher oxidizing potential such as $HO^{\bullet}$. Since at pH_0 6 the decomposition of O_3 into $HO^{\bullet}$ was mainly favored by PRM, and, in addition, pH decreased with time (Fig. S9), once PRM was eliminated the generation of $HO^{\bullet}$ diminished. In the case of the O_3/UVA system, despite the low absorbance of $O_3{\bullet}H_2O$ complexes at 365 nm (Axson et al., 2011), the use of high intensity LEDs favors the generation of $HO^{\bullet}$ by photolysis of O_3 (Figueredo et al., 2020), and this is clearly reflected in mineralization (32% DOC removal after 2 h). As discussed later (Section 3.2.2), at these conditions, OXAL formed during PRM oxidation by O_3/UVA can improve the decomposition of O_3 into $HO^{\bullet}$, also enhanced by other intermediates as it is the case of FOR (Yapsakli

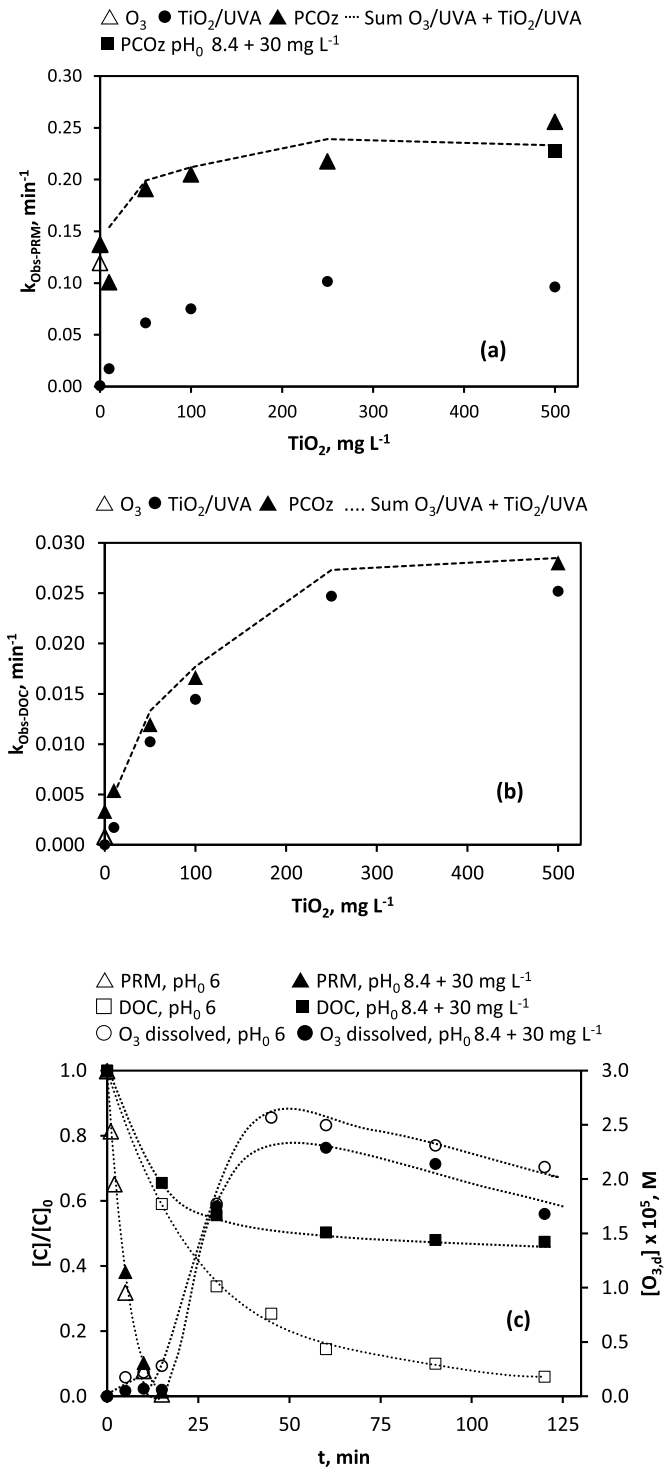

Fig. 5. PRM degradation by different processes in ultrapure water. (a) Influence of catalyst dose, ozone, UVA radiation, pH and IC content on $k_{Obs\text{-}PRM}$ (Eq. (1)); (b) influence of catalyst dose, ozone and UVA radiation in $k_{Obs\text{-}DOC}$ (Eq. (3)); (c) influence of pH and IC on PRM, DOC and dissolved time O_3 evolution by PCO_Z using 500 mg L^{-1} of TiO_2. Experimental conditions: $[PRM]_0$ 14 mg L^{-1} (~ 6.5 × 10^{-5} M), $[DOC]_0$ 9 mg L^{-1}, pH_0 6 (except where indicated), Q_g 15 L h^{-1}, $[O_{3g,\,in}]$ 10 mg L^{-1}, $I_{0,365\ nm} = 3.92\times10^{-5}$ Einstein $(L\ s)^{-1}$, $T = 20 \pm 2$ °C.

and Can, 2004). At pH_0 6, $k_{Obs\text{-}DOC}$ values of TiO_2/UVA and PCOz were similar at any TiO_2 dose, small differences correspond to the contribution to $k_{Obs\text{-}DOC}$ of O_3/UVA (Fig. 5b). Again, it is demonstrated no synergy between systems, h^+ being the main responsible of PRM mineralization by PCOz at pH < pH_{pzc}.

The effect of pH and alkalinity on DOC reduction by PCOz was significant. Thus, at pH 8.4 and 30 mg L^{-1} IC, after an initial evolution (up to 15 min) close to that experienced at pH_0 6 (Fig. 5c), the elimination rate of DOC slowed down to $k_{Obs\text{-}DOC} \sim 0.003\ min^{-1}$, value similar to the TiO_2/UVA system (Fig. 1b) and ten times lower than PCOz at pH_0 6 (Fig. 5b). During the first 15 min, regardless of the pH, as observed in Fig. 5c the concentration of ozone in the tank that fed the photoreactor was virtually zero. This means that, during this period, oxidant species are mainly generated by the decomposition of O_3 in the dark (favored by pH and the presence of PRM) and the photoexcitation of TiO_2 in the photoreactor, with no O_3-UVA or O_3-TiO_2/UVA interactions. After this period, the concentration of dissolved ozone in the tank (and, therefore, entering the photoreactor) increased, evolving similarly at pH_0 6 and 8.4 (30 mg L^{-1} IC). However, since at pH_0 8.4 almost no mineralization was attained, under these conditions it is suggested that, in addition to the null contribution of h^+ and the $HO^\bullet$ scavenging effect of IC, the contribution of $O_2^{\bullet-}$ generated from the reaction between electrons and dissolved O_2 at the catalyst surface to the decomposition of O_3 into $HO^\bullet$ (basis of the synergism between these systems) does not seem relevant.

Fig. 6 shows the concentration of carboxylic acids after 2 h. At pH_0 6, simple ozonation resulted in low carboxylic acids formation, consequence of the low reactivity of O_3 towards PRM intermediates and low O_3 decomposition into $HO^\bullet$ once PRM was degraded. Due to the ability of UVA to decompose O_3 into $HO^\bullet$, the O_3/UVA system led to a higher formation of carboxylic acids, identifying OXAL as the predominant. When TiO_2 was present, regardless of the presence of ozone (TiO_2/UVA and PCOz systems), at pH_0 6 participation of h^+ allowed almost complete mineralization and the accumulation of carboxylic acids was significantly reduced. On the contrary, during PCOz at pH_0 8.4 (30 mg L^{-1} of IC) OXAL accumulated in the reaction media due to the inhibition of reactions at the catalyst surface and because its low reactivity towards O_3 and $HO^\bullet$. Again, surface reactions are less decisive in the case of other carboxylic acids due to their much higher reactivity with $HO^\bullet$ or even $CO_3^{\bullet-}$. However, at pH_0 8.4 (30 mg L^{-1} of IC), after 2 h only ~ 35% of DOC in solution was in the form of carboxylic acids (25% of DOC as OXAL), which means that there must be other intermediates/final products whose degradation by PCOz is also adversely affected by increased pH and/or alkalinity.

3.2.2. Oxalic acid

Additional experiments were carried out by applying the different systems in the degradation of OXAL in ultrapure water. Two pH were tested, 3.5 and 8.4, in the latter case with/without 30 mg L^{-1} of IC. The evolution of the normalized remaining concentration of OXAL with time is shown in Fig. 7, and the evolution of pH in Fig. S10.

As seen in Fig. 7a (O_3 and O_3/UVA systems), at pH_0 3.5 the elimination of OXAL by simple ozonation was low (20% after 2 h), due to the low value of $k_{OXAL\text{-}O3}$ (< 0.04 $M^{-1}\ s^{-1}$, Hoigné and Bader, 1983) and low decomposition of O_3 into $HO^\bullet$ at these conditions. Combination of ozone with UVA (O_3/UVA) had a significant positive effect on OXAL elimination (> 95% after 2 h), as Moreira et al. (2016) also reported. On one hand, the high radiation intensity of 365 nm given by the LEDs favors the decomposition of O_3 into $HO^\bullet$ (as inferred from Fig. S11, that shows the evolution of dissolved ozone in the ozonation tank throughout the experiments), thus allowing the oxidation of a fraction of OXAL with concomitant formation of $CO_2^{-\bullet}$, that evolves to CO_2 and $O_2^{\bullet-}$. On the other hand, the superoxide radical propagates O_3 decomposition to finally yield $HO^\bullet$ (Garoma and Gurol, 2005; Vecitis et al., 2010). Concentration of H_2O_2 in solution was negligible (< 5 × 10^{-6} M, not shown). In any case, under acidic conditions the higher efficiency of O_3/UVA compared to O_3 cannot be associated to the O_3–H_2O_2 reaction (Merenyi et al., 2010).

At pH_0 8.4, regardless of the presence of IC, the benefit of combining O_3 and UVA in the elimination of OXAL disappeared, its oxidation rate being only slightly higher than for simple ozonation at pH_0 3.5. Since the increase on pH favors the decomposition of O_3 into $HO^\bullet$ Tomiyasu et al.,

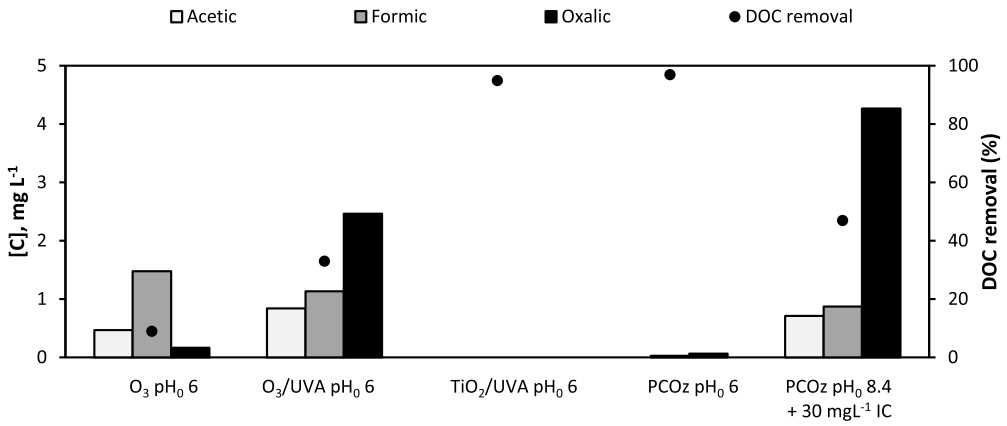

Fig. 6. Degradation of PRM by different processes in ultrapure water. Concentration of carboxylic acids and DOC removed (%) after 2 h. Experimental conditions: $[PRM]_0$ 14 mg L^{-1} (~ 6.5 × 10^{-5} M), $[DOC]_0$ 9 mg L^{-1}, $[TiO_2]$ 500 mg L^{-1}, Q_g 15 L h^{-1}, $[O_{3g,\ in}]$ 10 mg L^{-1}, $I_{0,365\ nm} = 3.92\times10^{-5}$ Einstein (L s)$^{-1}$, $T = 20 \pm 2$ °C.

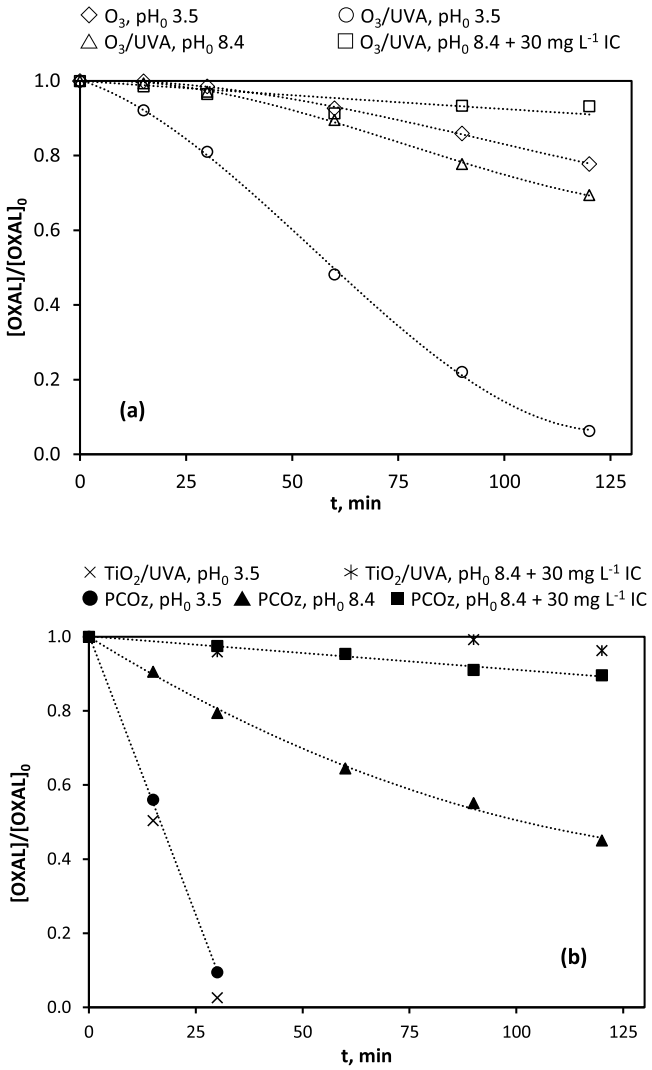

Fig. 7. Influence of pH and IC content on OXAL degradation in ultrapure water by O_3-based (a) and TiO_2-based (b) processes. Experimental conditions: $[OXAL]_0$ 3 × 10^{-4} M, $[DOC]_0$ ~ 7 mg L^{-1}, $[TiO_2]$ 500 mg L^{-1}, Q_g 15 L h^{-1}, $[O_{3g,\ in}]$ 10 mg L^{-1}, $I_{0,365\ nm} = 3.92\times10^{-5}$ Einstein (L s)$^{-1}$, $T = 20 \pm 2$ °C.

1985), these results can be explained based on the influence of pH on carbonate equilibria (Eq. (4)) and the reactivity of the different species present ($HCO_3^-/CO_3^=$ and OXAL) towards $HO^\bullet$. Thus, as the pH increases, given the relative low reactivity of OXAL (see Table S1), $HO^\bullet$ would mainly be consumed by $HCO_3^-/CO_3^=$, present or generated in the medium, through reactions ((5) and (6) (Garoma and Gurol, 2005).

Regarding systems that used TiO_2 (Fig. 7b), at pH_0 3.5, in agreement with the results obtained by Orge et al. (2015), the efficacy of TiO_2/UVA and PCOz was high and comparable (almost complete disappearance of OXAL in less than 30 min). In this situation, reactions occurring on the surface of the catalyst were mainly responsible for OXAL oxidation. At pH_0 8.4 and no IC addition, the efficiency of PCOz significantly decreased. However, the system still showed an important efficacy (55% OXAL removal after 2 h), likely due, once again, to the fast initial decrease of pH to neutral conditions (Fig. S10). At pH_0 8.4 and 30 mg L^{-1} IC (pH remained constant in all cases, Fig. S10) the conversion of OXAL by PCOz was very low and coincided with that of O_3/UVA (Fig. 7a). According to all these results, the PCOz system does not provide benefits in the degradation of OXAL compared to TiO_2/UVA (at acidic conditions) or O_3/UVA (higher pH and alkalinity), without observing any synergy between both systems.

3.2.3. *Secondary effluent from a MWWTP*

The matrix effect on PCOz efficacy was assessed treating the SE by the different systems. The PCOz system was also applied to the alkalinity-reduced SE at pH_0 7.5 and to the SE at pH_0 4 (no IC).

Fig. 8 shows the evolution of the normalized DOC concentration with time (Fig. 8a), and the concentration of carboxylic acids and % removal of DOC and absorbance at 254 nm (A_{254nm}) after 2 h (Fig. 8b). The evolution of dissolved ozone and H_2O_2 concentrations in the ozonation tank during these runs is shown in Fig. S12.

As seen in Fig. 8a, in the unaltered SE, the effectiveness of O_3 and O_3/UVA systems in DOC reduction was similar, UVA exerting a slight improvement from 60 min (20 and 25% after 2 h). At the pH of the SE, the decomposition of ozone into $HO^\bullet$ is expected to be relatively high, in agreement with the low dissolved ozone concentration observed, and favored by the presence of UVA (see Fig. S12a). Compared to ozone alone, the much lower concentration of dissolved ozone in the tank during O_3/UVA would indicate that intermediates or species generated from the photolysis of SE under UVA contribute to ozone decomposition in the dark, thus leading to a greater transformation of the EfOM. However, this effect was not sufficient to cause a significant effect on mineralization. For the systems that used TiO_2, while in the unaltered SE TiO_2/UVA was totally ineffective in DOC removal, 40% of mineralization was achieved by PCOz after 2 h, thus revealing a synergy between systems (see later). However, according to Fig. S12a, during O_3/UVA and PCOz the concentration of dissolved ozone in the ozonation tank

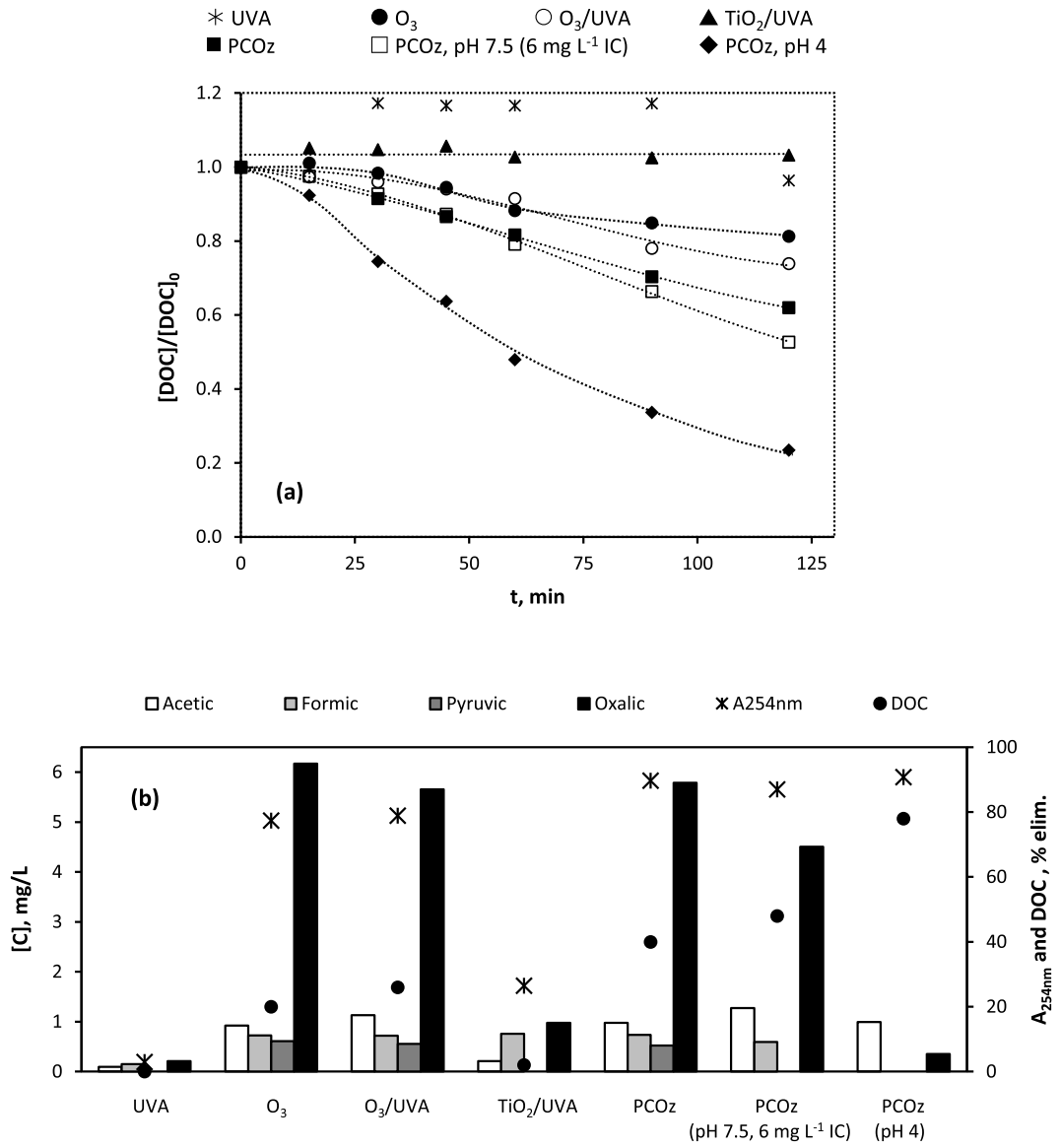

Fig. 8. Treatment of SE by different processes and conditions. (a) Evolution of normalized DOC with time; (b) concentration of carboxylic acids in solution and reduction (%) of A_{254nm} and DOC, after 2 h. Experimental conditions: $[DOC\text{-}SE]_0$ 10 - 12 mg L^{-1}, $A_{254nm,0}$ 0.26, $[IC]_0$ 25 mg L^{-1} and $pH_0 \sim 8.2$ except where indicated, $[TiO_2]$ 500 mg L^{-1}, Q_g 15 L h^{-1}, $[O_{3g,\ in}] \sim 10$ mg L^{-1}, $I_{0,365\ nm} = 3.92\times10^{-5}$ Einstein $(L\ s)^{-1}$, $T = 20 \pm 2$ °C.

(and hence, entering the photoreactor) kept lower than ~ 0.5 mg L^{-1} and evolved similarly, TiO_2 barely causing any effect in O_3 decomposition by PCOz.

Decreasing the initial pH and alkalinity of SE had a positive effect on DOC removal by PCOz. At pH_0 8.2 (25 mg L^{-1} IC), pH_0 7.5 (6 mg L^{-1} of IC) and pH_0 4 (no IC), after 2 h the DOC content was reduced by 40%, 48% and 80%, respectively. The fact that at pH_0 7.5 ($pH > pH_{pzc}$) and low IC the improvement was not significant (slight positive effect from 60 min), suggests that, under these conditions, the contribution of surface reactions to DOC mineralization is still low, and only the $HO^\bullet$ scavenging effect of $HCO_3^-/CO_3^=$ is reduced. At pH_0 4, that is, $pH < pH_{pzc}$ and no IC, the adsorption and subsequent oxidation of reaction intermediates by h^+ is favored, with a clear positive effect on DOC removal from the beginning. The higher efficiency of the process under acidic conditions results in lower ozone consumption per mg of DOC mineralized. Hence, after 2 h, in the unaltered SE (40% mineralization), 13 mg O_3 were consumed per mg DOC eliminated (3.2 mol O_3/mol DOC removed), whereas at pH_0 4 (80% mineralization) ozone consumption was reduced to 4 mg O_3/mg DOC (1 mol O_3/mol DOC removed).

At $pH_0 \geq 7.5$ the concentration of H_2O_2 in solution was $< 10^{-5}$ M, much lower than at pH_0 4 (see Fig. S12b), H_2O_2 being mainly formed from direct ozone reactions with the organic compounds present in SE. However, considering the pK_a 11.6 of H_2O_2, in acidic conditions, decomposition of O_3 into $HO^\bullet$ caused by HO_2^- would be minimal (Merenyi et al., 2010), as well as the contribution of H_2O_2 to $HO^\bullet$ from TiO_2/UVA (Nosaka and Nosaka, 2016).

As observed in Fig. 8b, given the high reactivity of O_3 towards aromatic rings with electron donor substituents (von Sonntag and von Gunten, 2012), all systems involving O_3 were very effective in reducing aromaticity, measured as A_{254nm}. For DIN content (not shown), regardless of the treatment and conditions applied, no variation was observed in $N\text{—}NH_4^+/N\text{—}NO_3^-$ content due to the negligible reactivity of NH_4^+ towards $HO^\bullet$ and O_3 (Hoigné and Bader, 1978). For the unaltered SE, after 2 h, OXAL was the most recalcitrant carboxylic acid in all the treatments applied, contributing to 20 – 25% of residual DOC in the case of ozone-based processes. A decrease in pH and alkalinity favored the oxidation of this acid by PCOz as expected, at pH_0 4 its contribution to final DOC being less than 5%.

According to the results obtained and discussed in this study, a clear synergy between O_3/UVA and TiO_2/UVA systems on DOC removal has only been observed when treating the SE, which points to the composition of the matrix as responsible for this synergy. To shed light on this matter, Fig. 9 compares the evolution of DOC and dissolved ozone in the tank that feeds the photoreactor during PCOz experiments performed with PRM (DOC_0 9 mg L^{-1}, pH 8.4 + 30 mg L^{-1} IC in ultrapure water), OXAL (DOC_0 7 mg L^{-1}, pH_0 8.4 + 30 mg L^{-1} IC in ultrapure water) and SE (DOC_0 10 – 12 mg L^{-1}, pH 8.2, 25 mg L^{-1} IC) working at same experimental conditions. In all cases, the concentration of H_2O_2 in the tank was very low ($< 10^{-5}$ M, not shown). As seen in Fig. 9, for PRM and SE, during the first 15 min the concentration of dissolved ozone in the tank was practically zero, that is, there is no ozone entering the photoreactor and no O_3-UVA or O_3-TiO_2/UVA interactions. After this period, the concentration of ozone increased but remained lower for SE (up to ~ 0.5 mg L^{-1} after 2 h), so O_3-UVA and O_3-TiO_2/UVA interactions would also be lower. Despite de above, DOC removal rate for SE resulted higher than for PRM and OXAL. These results could indicate that UVA photolysis of EfOM leads to the generation of reactive entities that promote the decomposition of ozone into HO•, allowing a faster transformation of the SE at the same time. As this transformation progresses UVA absorbance of SE will decrease, thus increasing the amount of radiation reaching the catalyst surface. It is worth mentioning that some authors have reported an increase of TiO_2 activity when treated with gaseous O_3 in the dark, attributed to the generation of OH groups at the catalyst surface (Zhang et al., 2019). In any case, no evidence has been found of direct interactions between O_3/UVA and TiO_2/UVA as responsible for the synergy observed in SE.

Finally, to establish the efficacy of PCOz in the elimination of microcontaminants, O_3 and PCOz experiments were replicated in unaltered SE spiked with CAF, PRM and p-CBA (100 μg L^{-1} each), all of them with low/medium reactivity towards O_3 and high and similar towards HO• (see Table S1). Evolution of pollutants concentration with time (Fig. S13a) reveals that, for both systems, the conversion rates followed the order of their reactivity with O_3. Considering the evolution of ozone in the inlet ($[O_{3g,in}]$) and outlet gas ($[O_{3g,out}]$) streams (Fig. S13b), the highest ozone consumption took place in the first 25 min of reaction, a period in which the removal of contaminants by O_3 or PCOz was practically complete. During this period, dissolved ozone entering the photoreactor was null (up to 15 min) or low ($< 5 \times 10^{-6}$ M) (see Fig. S12a), which means, once again, that there are hardly any O_3-UVA or O_3-TiO_2/UVA interactions. Fig. 10 shows the evolution of the normalized concentration of contaminants by O_3 and PCOz versus TOD/DOC_0. During simple ozonation there is an initial period of negligible target compounds degradation attributed to the fast initial consumption of O_3 by the matrix (absence of dissolved ozone, see Fig. S12a) together with the lower generation of HO• compared to PCOz. The higher efficiency of PCOz is reflected in the amount of ozone that needs to be transferred to remove a given percentage of pollutants. Thus, to reduce the concentration of the most refractory compounds by 90%, 1.75 mg O_3 (mg DOC_0)$^{-1}$ were required by PCOz, while simple ozonation needed 2.5 mg O_3 (mg DOC_0)$^{-1}$. These values are in agreement, although a bit lower, with those reported by Bertagna Silva et al. (2019) when applying O_3 and PCOz (3 BLB lamps, 8 W each, λ_{max} 365 nm, fluence rate 5.47 mW cm^{-2}) to remove the pesticide acetamiprid (ACMP, 100 μg L^{-1}), from secondary effluents of similar characteristics (pH 7.2 – 7.5, DOC_0 13 mg L^{-1}, alkalinity 208 - 275 mg L^{-1} as $CaCO_3$). However, some differences can be highlighted. Thus, until 50% of ACMP removal, the evolution of ACMP vs TOD/DOC_0 for both O_3 and PCOz was similar, whereas in this work (Fig. 10), clear differences were observed practically from the beginning. The reason might rely on the effectiveness of high-intensity UVA LEDs in promoting SE photolysis and HO• and other reactive species generation, much higher than for BLB lamps.

4. Conclusions

Working with different matrices and ozone transferred doses in the range of those commonly applied in WWTP, only when treating a real secondary effluent a synergy between O_3/UVA and TiO_2/UVA systems was observed. No evidence of direct interactions between systems has been found, which points to the composition of the matrix and its transformation along the treatment as responsible for this synergy. In a real secondary effluent, considering the ozone requirements, PCOz using UVA LEDs of high intensity could be an interesting strategy for the removal of micropollutants refractory to O_3, but not for DOC mineralization. In addition, the effective separation of catalyst particles after the treatment is the main issue to overcome. Hence, new studies on PCOz

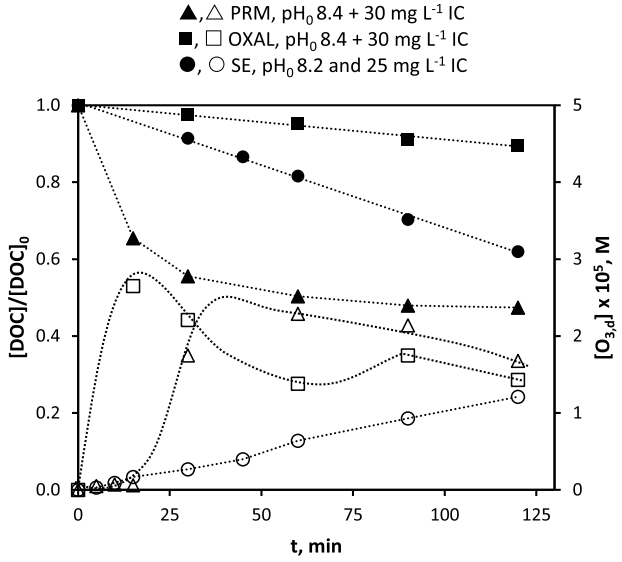

Fig. 9. Influence of the water matrix on the efficiency of PCOz. Evolution with time of normalized concentration of DOC (solid symbols) and dissolved ozone (open symbols) during photocalytic ozonation of PRM, OXAL or SE. Experimental conditions: $[DOC\text{-}PRM]_0$ 9 mg L^{-1}, $[DOC\text{-}OXAL]_0$ 7 mg L^{-1}, $[DOC\text{-}SE]_0$ 10 - 12 mg L^{-1}, $[TiO_2]$ 500 mg L^{-1}, Q_g 15 L h^{-1}, $[O_{3g,\ in}]$ 10 mg L^{-1}, $I_{0,365\ nm}$ = 3.92×10^{-5} Einstein (L s)$^{-1}$, T = 20 ± 2 °C.

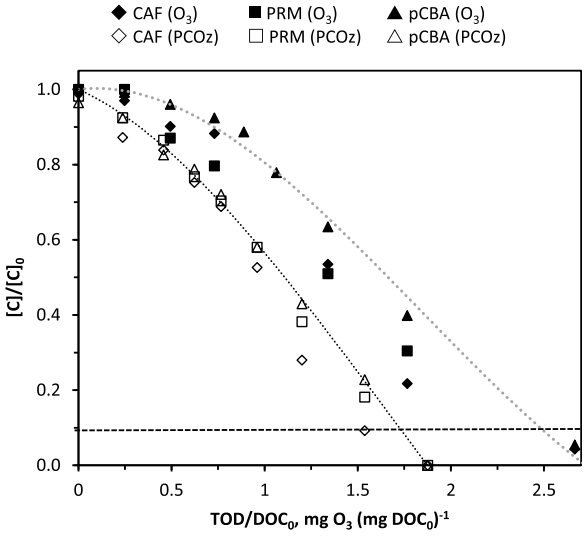

Fig. 10. Evolution of PRM, CAF and pCBA normalized concentration with the amount of ozone transferred per unit of DOC_0 during ozonation (solid symbols) and PCOz (open symbols) of SE. Experimental conditions: $[PRM]_0$ = $[CAF]_0$ = $[pCBA]_0$ = 100 μg L^{-1}, $[DOC\text{-}SE]_0$ 10 - 12 mg L^{-1}, pH_0 8.2, $[TiO_2]$ 500 mg L^{-1}, Q_g 15 L h^{-1}, $[O_{3g,\ in}]$ 10 mg L^{-1}, $I_{0,365\ nm}$ = 3.92×10^{-5} Einstein (L s)$^{-1}$, T = 20 ± 2 °C.

should focus on the use of supported materials.

Besides, the following specific conclusions can be addressed:

- At pH < pH_{pzc}, for compounds that do not adsorb onto the catalyst, both O_3/UVA and TiO_2/UVA individually contribute to their degradation. In terms of DOC mineralization, the efficiency of TiO_2/UVA is not affected by O_3, being h^+ the main species involved. At these conditions, no synergy or antagonism between systems is observed.
- At pH > pH_{pzc} the adsorption of organics with pK_a < pH_{pzc} is not favored, especially in presence of alkalinity, DOC mineralization by TiO_2/UVA being low or null. When combined with ozone (PCOz), both O_3/UVA and TiO_2/UVA contribute to some extent to the formation of $HO^{\bullet}$. However, only when a secondary effluent was treated a clear synergy between systems was deduced. This synergy seems to depend on the composition of the water matrix rather than on a direct interaction between systems.
- At the conditions applied, none of the systems tested was effective to oxidize N—NH_4^+.

Declaration of Competing Interest

The authors declare that they have no known competing financial interests or personal relationships that could have appeared to influence the work reported in this paper.

Acknowledgement

The authors thank the Ministerio de Economía y Competitividad of Spain and the European Funds for Regional Development (project CTQ2015/46944-R) and Agencia Estatal de Investigación of Spain (project PID2019-104429RB-I00/AEI/10.13039/501100011033) for the economic support. Manuel Alfredo Figueredo Fernández is grateful to the Ministerio de Economía y Competitividad of Spain for his predoctoral grant (Resolution 28/03/2017, BOE no. 217, of 08/09/2016, reference number BES-2016-078456).

Supplementary materials

Supplementary material associated with this article can be found, in the online version, at doi:10.1016/j.watres.2021.117727.

References

Alam, M.S., Rao, B.S.M.M., Janata, E., 2003. OH reactions with aliphatic alcohols: evaluation of kinetics by direct optical absorption measurement. A pulse radiolysis study. Radiat. Phys. Chem. 67, 723–728. https://doi.org/10.1016/S0969-806X(03)00310-4.

Autin, O., Hart, J., Jarvis, P., MacAdam, J., Parsons, S.A., Jefferson, B., 2013. The impact of background organic matter and alkalinity on the degradation of the pesticide metaldehyde by two advanced oxidation processes: UV/H_2O_2 and UV/TiO_2. Water Res. 47, 2041–2049. https://doi.org/10.1016/j.watres.2013.01.022 https://doi.org/.

Axson, J.L., Washenfelder, R.A., Kahan, T.F., Young, C.J., Vaida, V., Brown, S.S., 2011. Absolute ozone absorption cross section in the Huggins Chappuis minimum (350-470nm) at 296K. Atmos. Chem. Phys. 11, 11581–11590. https://doi.org/10.5194/acp-11-11581-2011.

Bader, H., Hoigné, J., 1981. Determination of ozone in water by the indigo method. Water Res. 15, 449–456. https://doi.org/10.1016/0043-1354(81)90054-3.

Bahnemann, D., Hart, E.J., 1982. Rate constants of the reaction of the hydrated electron and hydroxyl radical with ozone in aqueous solution. J. Phys. Chem. 86, 252–255. https://doi.org/10.1021/j100391a024.

Beltrán, F.J., Aguinaco, A., García-Araya, J.F., Oropesa, A., 2008. Ozone and photocatalytic processes to remove the antibiotic sulfamethoxazole from water. Water Res. 42, 3799–3808. https://doi.org/10.1016/j.watres.2008.07.019.

Beltrán, F.J., Rey, A., 2017. Solar or UVA-visible photocatalytic ozonation of water contaminants. Molecules 22, 1177. https://doi.org/10.3390/molecules22071177.

Bertagna Silva, D., Cruz-Alcalde, A., Sans, C., Giménez, J., Esplugas, S., 2019. Performance and kinetic modelling of photolytic and photocatalytic ozonation for enhanced micropollutants removal in municipal wastewaters. Appl. Catal. B Environ. 249, 211–217. https://doi.org/10.1016/j.apcatb.2019.02.072.

Bonsen, E.M., Schroeter, S., Jacobs, H., Broekaert, J.A.C., 1997. Photocatalytic degradation of ammonia with TiO_2 as photocatalyst in the laboratory and under the use of solar radiation. Chemosphere 35, 1431–1445. https://doi.org/10.1016/S0045-6535(97)00216-6.

Brame, J., Long, M., Li, Q., Alvarez, P., 2015. Inhibitory effect of natural organic matter or other background constituents on photocatalytic advanced oxidation processes: mechanistic model development and validation. Water Res. 84, 362–371. https://doi.org/10.1016/j.watres.2015.07.044.

Burek, B.O., Timm, J., Bahnemann, D.W., Bloh, J.Z., 2019. Kinetic effects and oxidation pathways of sacrificial electron donors on the example of the photocatalytic reduction of molecular oxygen to hydrogen peroxide over illuminated titanium dioxide. Catal. Today 335, 354–364. https://doi.org/10.1016/j.cattod.2018.12.044.

Buxton, G.V., Elliot, A.J., 1986. Rate constant for reaction of hydroxyl radicals with bicarbonate ions. Int. J. Radiat. Appl. Instrumentation. Part 27, 241–243. https://doi.org/10.1016/1359-0197(86)90059-7.

Buxton, G.V., Greenstock, C.L., Helman, W.P., Ross, A.B., 1988. Critical Review of rate constants for reactions of hydrated electrons, hydrogen atoms and hydroxyl radicals (·OH/·O−) in Aqueous Solution. J. Phys. Chem. Ref. Data 17, 513–886. https://doi.org/10.1063/1.555805.

Cederbaum, A.I., Qureshi, A., Cohen, G., 1983. Production of formaldehyde and acetone by hydroxyl-radical generating systems during the metabolism of tertiary butyl alcohol. Biochem. Pharmacol. 32, 3517–3524. https://doi.org/10.1016/0006-2952(83)90297-6.

Chuang, L.C., Luo, C.H., Huang, S.W., Wu, Y.C., Huang, Y.C., 2011. Photocatalytic degradation mechanism and kinetics of caffeine in aqueous suspension of nano-TiO_2. Adv. Mater. Res. 214, 97–102. https://doi.org/10.4028/www.scientific.net/AMR.214.97.

Dalmázio, I., Santos, L.S., Lopes, R.P., Eberlin, M.N., Augusti, R., 2005. Advanced oxidation of caffeine in water: on-line and real-time monitoring by electrospray ionization mass spectrometry. Environ. Sci. Technol. 39, 5982–5988. https://doi.org/10.1021/es047985v.

Dolamic, I., Bürgi, T., 2007. Photocatalysis of dicarboxylic acids over TiO_2: an in situ ATR-IR study. J. Catal. 248, 268–276. https://doi.org/10.1016/j.jcat.2007.03.020.

Farner Budarz, J., Turolla, A., Piasecki, A.F., Bottero, J.Y., Antonelli, M., Wiesner, M.R., 2017. Influence of aqueous inorganic anions on the reactivity of nanoparticles in TiO_2 photocatalysis. Langmuir 33, 2770–2779. https://doi.org/10.1021/acs.langmuir.6b04116.

Fathinia, M., Khataee, A., Aber, S., Naseri, A., 2016. Development of kinetic models for photocatalytic ozonation of phenazopyridine on TiO_2 nanoparticles thin film in a mixed semi-batch photoreactor. Appl. Catal. B Environ. 184, 270–284. https://doi.org/10.1016/j.apcatb.2015.11.033.

Figueredo, M.A., Rodríguez, E.M., Checa, M., Beltran, F.J., 2019. Ozone-based advanced oxidation processes for primidone removal in water using simulated solar radiation and TiO_2 or WO_3 as photocatalyst. Molecules 24, 1728. https://doi.org/10.3390/molecules24091728 https://doi.org/doi:

Figueredo, M., Rodríguez, E.M., Rivas, J., Beltrán, F.J., 2020. Kinetic model basis of ozone/light-based advanced oxidation processes: a pseudoempirical approach. Environ. Sci. Water Res. Technol. 6, 1176–1185. https://doi.org/10.1039/d0ew00064g.

Garoma, T., Gurol, M.D., 2005. Modeling aqueous ozone/UV process using oxalic acid as probe chemical. Environ. Sci. Technol. 39, 7964–7969. https://doi.org/10.1021/es050878w.

Hoigne, J., Bader, H., 1978. Ozonation of water: kinetics of oxidation of ammonia by ozone and hydroxyl radicals. Environ. Sci. Technol. 12, 79–84. https://doi.org/10.1021/es60137a005.

Hoigné, J., Bader, H., 1983. Rate constants of reactions of ozone with organic and inorganic compounds in water—II. Water Res. 17, 185–194. https://doi.org/10.1016/0043-1354(83)90099-4.

Huang, L., Li, L., Dong, W., Liu, Y., Hou, H., 2008. Removal of ammonia by OH radical in aqueous phase. Environ. Sci. Technol. 42, 8070–8075. https://doi.org/10.1021/es8008216.

Hug, S.J., Sulzberger, B., 1994. In situ fourier transform infrared spectroscopic evidence for the formation of several different surface complexes of oxalate on TiO_2 in the aqueous phase. Langmuir 10, 3587–3597. https://doi.org/10.1021/la00022a036.

Ivanova, I., Mendive, C.B., Bahnemann, D., 2016. The role of nanoparticulate agglomerates in TiO_2 photocatalysis: degradation of oxalic acid. J. Nanoparticle Res. 18, 1–13. https://doi.org/10.1007/s11051-016-3495-x.

Jallouli, N., Pastrana-Martínez, L.M., Ribeiro, A.R., Moreira, N.F.F., Faria, J.L., Hentati, O., Silva, A.M.T., Ksibi, M., 2018. Heterogeneous photocatalytic degradation of ibuprofen in ultrapure water, municipal and pharmaceutical industry wastewaters using a TiO_2/UV-LED system. Chem. Eng. J. 334, 976–984. https://doi.org/10.1016/j.cej.2017.10.045.

Jefferson, B., Jarvis, P., Bhagianathan, G.K., Smith, H., Autin, O., Goslan, E.H., MacAdam, J., Carra, I., 2016. Effect of elevated UV dose and alkalinity on metaldehyde removal and THM formation with UV/TiO_2 and UV/H_2O_2. Chem. Eng. J. 288, 359–367. https://doi.org/10.1016/j.cej.2015.11.071 https://doi.org/.

Kim, W., Tachikawa, T., Moon, G.H., Majima, T., Choi, W., 2014. Molecular-level understanding of the photocatalytic activity difference between anatase and rutile nanoparticles. Angew. Chem. - Int. Ed. 53, 14036–14041. https://doi.org/10.1002/anie.201406625.

Kominami, H., Furusho, A., Murakami, S.Y., Inoue, H., Kera, Y., Ohtani, B., 2001. Effective photocatalytic reduction of nitrate to ammonia in an aqueous suspension of metal-loaded titanium(IV) oxide particles in the presence of oxalic acid. Catal. Lett. 76, 31–34. https://doi.org/10.1023/A:1016771908609.

Kosanić, M.M., 1998. Photocatalytic degradation of oxalic acid over TiO_2 power. J. Photochem. Photobiol. A Chem. 119, 119–122. https://doi.org/10.1016/S1010-6030(98)00407-9.

Kosmulski, M., 2009. pH-dependent surface charging and points of zero charge. IV. Update and new approach. J. Colloid Interface Sci. 337, 439–448. https://doi.org/10.1016/j.jcis.2009.04.072.

Krýsa, J., Waldner, G., Měšťánková, H., Jirkovský, J., Grabner, G., 2006. Photocatalytic degradation of model organic pollutants on an immobilized particulate TiO_2 layer. Roles of adsorption processes and mechanistic complexity. Appl. Catal. B Environ. 64, 290–301. https://doi.org/10.1016/j.apcatb.2005.11.007.

Lado Ribeiro, A.R., Moreira, N.F.F., Li Puma, G., Silva, A.M.T., 2019. Impact of water matrix on the removal of micropollutants by advanced oxidation technologies. Chem. Eng. J. 363, 155–173. https://doi.org/10.1016/j.cej.2019.01.080.

Lee, E., Glover, C.M., Rosario-Ortiz, F.L., 2013. Photochemical formation of hydroxyl radical from effluent organic matter: role of composition. Environ. Sci. Technol. 47, 12073–12080. https://doi.org/10.1021/es402491t.

Li, L., Sillanpää, M., Risto, M., 2016. Influences of water properties on the aggregation and deposition of engineered titanium dioxide nanoparticles in natural waters. Environ. Pollut. 219, 132–138. https://doi.org/10.1016/j.envpol.2016.09.080 https://doi.org/.

Maghsoodi, M., Jacquin, C., Teychené, B., Heran, M., Tarabara, V.V., Lesage, G., Snow, S. D., 2019. Emerging investigator series: photocatalysis for MBR effluent post-treatment: assessing the effects of effluent organic matter characteristics. Environ. Sci. Water Res. Technol. 5, 482–494. https://doi.org/10.1039/c8ew00734a.

Márquez, G., Rodríguez, E.M., Beltrán, F.J., Álvarez, P.M., 2014. Solar photocatalytic ozonation of a mixture of pharmaceutical compounds in water. Chemosphere 113, 71–78. https://doi.org/10.1016/j.chemosphere.2014.03.093.

Masschelein, W., Denis, M., Ledent, R., 1977. Spectrophotometric determination of residual hydrogen peroxide. Water Sew. Work 124, 69–72.

Mecha, A.C., Chollom, M.N., 2020. Photocatalytic ozonation of wastewater: a review. Environ. Chem. Lett. 18, 1491–1507. https://doi.org/10.1007/s10311-020-01020-x.

Mehrjouei, M., Müller, S., Möller, D., 2015. A review on photocatalytic ozonation used for the treatment of water and wastewater. Chem. Eng. J. https://doi.org/10.1016/j.cej.2014.10.112.

Mendive, C.B., Blesa, M.A., Bahnemann, D., 2007. The adsorption and photodegradation of oxalic acid at the TiO_2 surface. Water Sci. Technol. 55, 139–145. https://doi.org/10.2166/wst.2007.398.

Merényi, G., Lind, J., Naumov, S., Sonntag, C.Von, 2010. Reaction of ozone with hydrogen peroxide (peroxone process): a revision of current mechanistic concepts based on thermokinetic and quantum-chemical considerations. Environ. Sci. Technol. 44, 3505–3507. https://doi.org/10.1021/es100277d.

Moreira, N.F.F., Orge, C.A., Ribeiro, A.R., Faria, J.L., Nunes, O.C., Pereira, M.F.R., Silva, A.M.T., 2015. Fast mineralization and detoxification of amoxicillin and diclofenac by photocatalytic ozonation and application to an urban wastewater. Water Res. 87, 87–96. https://doi.org/10.1016/j.watres.2015.08.059.

Moreira, N.F.F., Sousa, J.M., Macedo, G., Ribeiro, A.R., Barreiros, L., Pedrosa, M., Faria, J.L., Pereira, M.F.R., Castro-Silva, S., Segundo, M.A., Manaia, C.M., Nunes, O. C., Silva, A.M.T., 2016. Photocatalytic ozonation of urban wastewater and surface water using immobilized TiO_2 with LEDs: micropollutants, antibiotic resistance genes and estrogenic activity. Water Res. 94, 10–22. https://doi.org/10.1016/j.watres.2016.02.003.

Neta, P., Huie, R.E., Ross, A.B., 1988. Rate constants for reactions of inorganic radicals in aqueous solution. J. Phys. Chem. Ref. Data 17, 1027–1284. https://doi.org/10.1063/1.555808.

Nosaka, Y., Nosaka, A., 2016. Understanding hydroxyl radical (•OH) generation processes in photocatalysis. ACS Energy Lett. 1, 356–359. https://doi.org/10.1021/acsenergylett.6b00174.

Nosaka, Y., Nosaka, A.Y., 2017. Generation and detection of reactive oxygen species in photocatalysis. Chem. Rev. 117, 11302–11336. https://doi.org/10.1021/acs.chemrev.7b00161.

Ohtani, B., Prieto-Mahaney, O.O., Li, D., Abe, R., 2010. What is degussa (Evonik) P25 crystalline composition analysis, reconstruction from isolated pure particles and photocatalytic activity test. J. Photochem. Photobiol. A Chem. 216, 179–182. https://doi.org/10.1016/j.jphotochem.2010.07.024 https://doi.org/https://doi.org/.

Orge, C.A., Pereira, M.F.R., Faria, J.L., 2015. Photocatalytic ozonation of model aqueous solutions of oxalic and oxamic acids. Appl. Catal. B Environ. 174–175, 113–119. https://doi.org/10.1016/j.apcatb.2015.02.038.

Park, J.H., Kim, S.G., Park, S.S., Hong, S.S., Lee, G.D., 2006. Photocatalytic oxidation and decomposition of acetic acid over TiO_2, TS-1 and Ti-MCM-41 catalysts. Mater. Sci. Forum 510–511, 34–37. https://doi.org/10.4028/www.scientific.net/msf.510-511.34.

Perez Holmberg, J., Ahlberg, E., Bergenholtz, J., Hassellöv, M., Abbas, Z., 2013. Surface charge and interfacial potential of titanium dioxide nanoparticles: experimental and theoretical investigations. J. Colloid Interface Sci. 407, 168–176. https://doi.org/10.1016/j.jcis.2013.06.015.

Real, F.J., Javier Benitez, F., Acero, J.L., Sagasti, J.J.P., Casas, F., 2009. Kinetics of the chemical oxidation of the pharmaceuticals primidone, ketoprofen, and diatrizoate in ultrapure and natural waters. Ind. Eng. Chem. Res. 48, 3380–3388. https://doi.org/10.1021/ie801762p.

Rimoldi, L., Meroni, D., Falletta, E., Pifferi, V., Falciola, L., Cappelletti, G., Ardizzone, S., 2017. Emerging pollutant mixture mineralization by TiO_2 photocatalysts. The role of the water medium. Photochem. Photobiol. Sci. 16, 60–66. https://doi.org/10.1039/c6pp00214e.

Rodríguez, E.M., Fernández, G., Klamerth, N., Maldonado, M.I., Álvarez, P.M., Malato, S., 2010. Efficiency of different solar advanced oxidation processes on the oxidation of bisphenol A in water. Appl. Catal. B Environ. 95, 228–237. https://doi.org/10.1016/j.apcatb.2009.12.027.

Rodríguez, E.M., Márquez, G., Tena, M., Álvarez, P.M., Beltrán, F.J., 2015. Determination of main species involved in the first steps of TiO_2 photocatalytic degradation of organics with the use of scavengers: the case of ofloxacin. Appl. Catal. B Environ. 178, 44–53. https://doi.org/10.1016/j.apcatb.2014.11.002.

Rosal, R., Gonzalo, M.S., Rodríguez, A., García-Calvo, E., 2009. Ozonation of clofibric acid catalyzed by titanium dioxide. J. Hazard. Mater. 169, 411–418. https://doi.org/10.1016/j.jhazmat.2009.03.111.

Schneider, J.T., Firak, D.S., Ribeiro, R.R., Peralta-Zamora, P., 2020. Use of scavenger agents in heterogeneous photocatalysis: truths, half-truths, and misinterpretations. Phys. Chem. Chem. Phys. 22, 15723–15733. https://doi.org/10.1039/d0cp02411b.

Shi, X., Dalal, N.S., Jain, A.C., 1991. Antioxidant behaviour of caffeine: efficient scavenging of hydroxyl radicals. Food Chem. Toxicol. 29, 1–6. https://doi.org/10.1016/0278-6915(91)90056-D.

Šuligoj, A., Kete, M., Černigoj, U., Fresno, F., Lavrenčič Štangar, U., 2021. Synergism in TiO_2 photocatalytic ozonation for the removal of dichloroacetic acid and thiacloprid. Environ. Res. 197 https://doi.org/10.1016/j.envres.2021.110982.

Tomiyasu, H., Fukutomi, H., Gordon, G., 1985. Kinetics and mechanism of ozone decomposition in basic aqueous solution. Inorg. Chem. 24, 2962–2966. https://doi.org/10.1021/ic00213a018.

Tong, A.Y.C., Braund, R., Warren, D.S., Peake, B.M., 2012. TiO_2-assisted photodegradation of pharmaceuticals- a review. Cent. Eur. J. Chem. 10, 989–1027. https://doi.org/10.2478/s11532-012-0049-7.

Vecitis, C.D., Lesko, T., Colussi, A.J., Hoffmann, M.R., 2010. Sonolytic decomposition of aqueous bioxalate in the presence of ozone. J. Phys. Chem. A 114, 4968–4980. https://doi.org/10.1021/jp9115386.

von Sonntag, C., von Gunten, U., 2012. Chemistry of Ozone in Water and Wastewater Treatment: from Basic Principles to Applications, Water Intelligence Online. IWA Publishing, London. https://doi.org/10.2166/9781780400839.

Wang, H., Adesina, A.A., 1997. Photocatalytic causticization of sodium oxalate using commercial TiO2 particles. Appl. Catal. B Environ. 14, 241–247. https://doi.org/10.1016/S0926-3373(97)00026-X.

Wang, P., 2017. Aggregation of TiO_2 nanoparticles in aqueous media: effects of pH, ferric ion and humic acid. Int. J. Environ. Sci. Nat. Resour. 1, 157–162. https://doi.org/10.19080/ijesnr.2017.01.555575.

Weisz, A.D., García Rodenas, L., Morando, P.J., Regazzoni, A.E., Blesa, M.A., 2002. FTIR study of the adsorption of single pollutants and mixtures of pollutants onto titanium dioxide in water: oxalic and salicylic acids. Catal. Today 76, 103–112. https://doi.org/10.1016/S0920-5861(02)00210-9.

Wojnárovits, L., Tóth, T., Takács, E., 2020. Rate constants of carbonate radical anion reactions with molecules of environmental interest in aqueous solution: a review. Sci. Total Environ. 717 (2020), 137219 https://doi.org/10.1016/j.scitotenv.2020.137219.

Yapsakli, K., Can, Z.S., 2004. Interaction of ozone with formic acid: a system which supresses the scavenging effect of HCO_3^-/CO_3^{2-}. Water Qual. Res. J. Canada 39, 140–148. https://doi.org/10.2166/wqrj.2004.021.

Zhang, Y., Chen, Y., Westerhoff, P., Crittenden, J., 2009. Impact of natural organic matter and divalent cations on the stability of aqueous nanoparticles. Water Res. 43, 4249–4257. https://doi.org/10.1016/j.watres.2009.06.005.

Zhang, F., Hong, B., Zhao, W., Yang, Y., Bao, J., Gao, C., Sun, S., 2019. Ozone modification as an efficient strategy for promoting the photocatalytic effect of TiO_2 for air purification. Chem. Commun. 55, 3757–3760. https://doi.org/10.1039/c9cc00814d.

Zhou, H., Lian, L., Yan, S., Song, W., 2017. Insights into the photo-induced formation of reactive intermediates from effluent organic matter: the role of chemical constituents. Water Res. 112, 120–128. https://doi.org/10.1016/j.watres.2017.01.048.

Zhu, X., Castleberry, S.R., Nanny, M.A., Butler, E.C., 2005. Effects of pH and catalyst concentration on photocatalytic oxidation of aqueous ammonia and nitrite in titanium dioxide suspensions. Environ. Sci. Technol. 39, 3784–3791. https://doi.org/10.1021/es0485715.